Title

Enhancing myelin renewal reverses cognitive dysfunction in a murine model of Alzheimer's disease

Journal

Neuron, 109(14)

ISSN

0896-6273

Authors

Chen, Jing-Fei
Liu, Kun
Hu, Bo
et al.

Publication Date

2021-07-01

DOI

10.1016/j.neuron.2021.05.012

Peer reviewed

HHS Public Access

Author manuscript

Neuron. Author manuscript; available in PMC 2022 July 21.

Published in final edited form as:

Neuron. 2021 July 21; 109(14): 2292–2307.e5. doi:10.1016/j.neuron.2021.05.012.

Enhancing myelin renewal reverses cognitive dysfunction in a murine model of Alzheimer's disease

Jing-Fei Chen[1,6], **Kun Liu**[1,6], **Bo Hu**[2,6], **Rong-Rong Li**[2], **Wendy Xin**[3], **Hao Chen**[4], **Fei Wang**[1], **Lin Chen**[1], **Rui-Xue Li**[1], **Shu-Yu Ren**[1], **Lan Xiao**[1,*], **Jonah R. Chan**[3,*], **Feng Mei**[1,5,*]

[1]Brain and Intelligence Research Key Laboratory of Chongqing Education Commission, Department of Histology and Embryology, Third Military Medical University, Chongqing 400038, China.

[2]Department of Physiology, Chongqing Key Laboratory of Neurobiology, Brain and Intelligence Research Key Laboratory of Chongqing Education Commission, Third Military Medical University, Chongqing 400038, China.

[3]UCSF Weill Institute for Neurosciences, Department of Neurology, University of California at San Francisco, San Francisco, CA 94158, USA.

[4]Experimental center of Basic Medicine, College of Basic Medical Sciences, Third Military Medical University, Chongqing 400038, China.

[5]Lead contact

[6]These authors contributed equally

SUMMARY

Severe cognitive decline is a hallmark of Alzheimer's disease (AD). In addition to grey matter loss, significant white matter pathology has been identified in AD patients. Here, we characterized the dynamics of myelin generation and loss in the APP/PS1 mouse model of AD. Unexpectedly, we observed a dramatic increase in the rate of new myelin formation in APP/PS1 mice, reminiscent of the robust oligodendroglial response to demyelination. Despite this increase, overall levels of myelination are decreased in the cortex and hippocampus of APP/PS1 mice and postmortem AD tissue. Genetically or pharmacologically enhancing myelin renewal, by oligodendroglial deletion of the muscarinic M1 receptor or systemic administration of the pro-myelinating drug clemastine, improved the performance of APP/PS1 mice in memory-related tasks and increased hippocampal sharp wave ripples. Taken together, these results demonstrate the potential of enhancing myelination as a therapeutic strategy to improve AD-related cognitive impairment.

*Correspondence: jonah.chan@ucsf.edu (J.R.C.); xiaolan35@hotmail.com (L.X.); meif@tmmu.edu.cn (F. M.).

Author contributions: J.F.C., K.L., B.H., R.R.L., H.C., F.W., L.C., R.X.L. and S.Y.R., performed experiments. J.F.C., B.H., R.X.L., L.X., J.R.C. and F.M. provided reagents. J.F.C., K.L., B.H., L.X., W.X., J.R.C. and F.M., provided intellectual contributions. J.F.C., K.L., B.H., X.L., W.X., J.R.C. and F.M. analyzed the data and wrote the paper. All authors read and approved the manuscript.

Declaration of Interests: Authors declare no competing interests.

Graphical Abstract

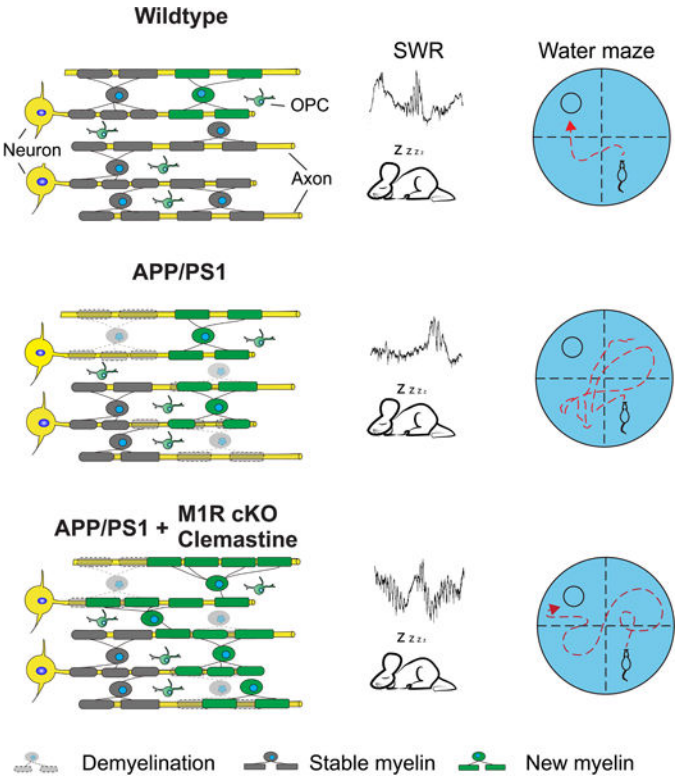

eTOC :

Chen et al., demonstrate myelin formation is increased in APP/PS1 mice, that is reminiscent of a regenerative response to extensive demyelination, and pro-myelinating strategies enhance myelin renewal in AD mice and rescues AD-related cognitive deficits and increases hippocampal sharp wave ripples.

INTRODUCTION

Alzheimer's disease (AD) is an age-related neurodegenerative disease that presents with progressive cognitive decline, for which effective treatments have remained elusive (Long and Holtzman, 2019; Scheltens et al., 2016). Though AD-related cognitive impairment is thought to be the result of neuronal dysfunction and degeneration (De Strooper and Karran, 2016; Heneka et al., 2015; Murray et al., 2011), significant disruptions in glial function have also been reported in patients with AD (Arranz and De Strooper, 2019; Behrendt et al., 2013; Grubman et al., 2019; Henstridge et al., 2019). In particular, histological and functional imaging studies have found significant alterations in the white matter structure of AD patients (Alzheimer, 1911; Benitez et al., 2014; Brun and Englund, 1986; Luo et al., 2019; Migliaccio et al., 2012; Moghekar et al., 2012; Phillips et al., 2016; Ringman et al., 2007; Roseborough et al., 2017; Stricker et al., 2009; Taylor et al., 2017; Bartzokis., 2003). White matter is composed of axons and myelin, a fatty sheath produced by oligodendrocytes that increases axonal conductance and is critical for neuronal signaling. Whether these white

matter abnormalities actively contribute to the symptomology and/or progression of AD, or are simply secondary to neuronal degeneration, is currently unclear.

Oligodendrocytes and the myelin sheaths they produce wrap axons to optimize conduction velocity and provide neurons with numerous metabolic and trophic factors required for their survival (Fünfschilling et al., 2012; Lee et al., 2012; Mot et al., 2018). Mature oligodendrocytes and individual myelin sheaths, once generated, are mostly stable in the adult and aging brain. However, recent studies have shown that new myelin is continuously generated via the differentiation of oligodendrocyte precursor cells (OPCs) throughout life (Hill et al., 2018; Hughes et al., 2018; Wang et al., 2020), and that this ongoing addition of oligodendrocytes and myelin is required for a range of cognitive tasks (Xin and Chan, 2020), including the preservation of fear and spatial memory (Pan et al., 2020; Steadman et al., 2020). During aging, myelin generation decreases considerably, which seems to contribute to declining cognitive function in aged mice (Wang et al., 2020). These findings raise the possibility that altered myelin dynamics may partially underlie the cognitive deficits experienced by patients with AD.

Multiple lines of evidence indicate that myelin and oligodendroglia are significantly altered in AD-related pathology. Single-cell transcriptomic analyses have detected significant gene expression changes in oligodendrocyte lineage cells from early-stage AD patient brains (Mathys et al., 2019; Zhou et al., 2020) and myelin abnormalities have been identified in AD model brains (Desai et al., 2010; Desai et al., 2009; Mitew et al., 2010; Schmued et al., 2013). For example, Aβ deposition causes focal demyelination and senescence-like changes in OPCs, while the average rate of OPC proliferation was increased in transgenic AD mouse brains, hinting that both aberrant myelin degeneration and remyelination may be occurring in the AD brains (Kang et al., 2013; Zhang et al., 2019b). Thus, understanding AD-related changes in myelin dynamics may require genetic cell-lineage tracing to track the fate of pre-existing and newly formed myelin over time.

Here, we report an accelerated degeneration of pre-existing myelin sheaths that is coincident with a significant increase in oligodendrogenesis and myelination in the APP/PS1 transgenic mouse brains, resulting in net myelin loss. Enhancing myelin renewal by deleting the muscarinic M1 receptor (M1R) in OPCs, or treatment with the pro-myelinating drug clemastine, significantly improved the performance of APP/PS1 mice in memory-related tasks and increased the occurrence and peak frequency of hippocampal sharp wave ripples. Together, these results demonstrate the potential of enhancing myelination as a therapeutic strategy to improve AD-related cognitive impairment.

RESULTS

Myelin formation and degeneration are both elevated in APP/PS1 mice

Recent studies have shown that new myelin is continuously added in the adult brain, even well into aging (Hill et al., 2018; Wang et al., 2020). Enhancing new myelin formation in aged mice improves spatial memory, whereas preventing new myelin formation in middle-aged mice impairs spatial memory (Wang et al., 2020). Therefore, we hypothesized that the rate of myelin formation may be decreased in AD. To visualize myelin formation, we used

the NG2-CreERT; Tau-mGFP mouse line to label newly formed myelin sheaths (Mei et al., 2016; Young et al., 2013). Recombination of the Tau-mGFP allele is induced by tamoxifen in NG2-expressing OPCs, but since Tau is highly expressed by mature oligodendrocytes and very low in OPCs, membrane-bound GFP (mGFP) will only be present in oligodendrocytes and myelin sheaths formed after tamoxifen administration (Young et al., 2013). APP/PS1; NG2-CreERT; Tau-mGFP mice and littermate controls were given tamoxifen at 7 months of age, close to when cognitive defects first emerge in APP/PS1 mice (Reiserer et al., 2007), then perfused for histology after three months (Figure 1A). Unexpectedly, we observed significantly more mGFP-positive (mGFP+) myelin sheaths in the corpus callosum, cortex, and hippocampus of APP/PS1 mice than in controls (Figures 1B–E).

A large increase in myelination typically occurs following a demyelinating injury (Franklin and Ffrench-Constant, 2008; Franklin and Goldman, 2015), which suggests that the increased myelin formation in APP/PS1 mice may be an endogenous response to myelin degeneration. To track the fate of pre-existing myelin sheaths, we crossed in the PLP-CreERT; mT/mG alleles to label myelin sheaths that were already formed at the time of tamoxifen administration (Figure 1F). PLP is a myelin-associated protein that is expressed only by mature oligodendrocytes; thus, in PLP-CreERT; mT/mG mice, pre-existing oligodendrocytes and myelin sheaths will express mGFP upon tamoxifen-induced recombination. APP/PS1; PLP-CreERT; mT/mG mice and littermate controls were treated with tamoxifen at 2–4 months of age and perfused for histology at 13 months. Relative to controls, APP/PS1 mice had significantly lower levels of mGFP+ area in cortex and hippocampus, indicating extensive loss of pre-existing myelin sheaths relative to controls (Figures 1G–I). To examine whether there is a relationship between Aβ plaques – a pathological hallmark of AD that is recapitulated in APP/PS1 mice (Gordon et al., 2001) – we examined the pattern of myelination around Aβ deposits in APP/PS1 mice (Figure S1A). Aβ deposits appeared to induce focal demyelination and inflammation, indicated by the absence of mGFP+ myelin sheaths and the presence of activated Iba1-positive microglia around the plaques (Figure S1B). However, Aβ deposits were only present in approximately 1% of the mGFP+ areas in 8-month-old APP/PS1 brains (Figure S1A), implying that the degeneration of pre-existing myelin also occurred extensively in areas devoid of Aβ deposition. Additionally, upon further examination of myelin renewal, we found the amount of newly formed myelin (i.e.,mGFP+ myelin internodes in the NG2-CreERT; Tau-mGFP line) was comparable in regions adjacent to, or further away from, Aβ deposits (Figure S1C). These results indicate that the degeneration of myelin in the APP/PS1 mice is not exclusively attributable to Aβ plaques and that myelin renewal does not tend to occur in these regions. Therefore, the alteration in myelin dynamics in the APP/PS1 mice is likely the result of a different, as of yet unidentified, mechanism.

To determine whether the newly generated myelin sheaths are transiently formed or maintained over time, we immunostained for myelin basic protein (MBP) in APP/PS1; PLP-CreERT; mT/mG mice that were treated with tamoxifen at 2–4 months and sacrificed at 13 months (Figures S1D and S1E). In these mice, myelin sheaths that existed at the time of recombination would be double positive for mGFP and MBP (mGFP+ MBP+, pseudo-colored blue), whereas sheaths that were formed subsequent to tamoxifen treatment would only be positive for MBP (mGFP- MBP+, pseudo-colored red). We observed an almost two-

fold increase in the amount of myelin sheaths generated after 2–4 months of age in APP/PS1 mice, which suggests that the increased rate of myelin formation did result in the stable accumulation of new myelin sheaths (Figures S1F–S1H).

Extensive myelin loss in APP/PS1 mice and individuals with AD

Since both myelin formation and myelin degeneration were significantly elevated in APP/PS1 mice, we quantified the overall levels of MBP by immunostaining and western blot to determine whether these processes resulted in a net change in myelination. At 4 months of age, MBP expression in the cortex and hippocampus of APP/PS1 mice were comparable to controls but were decreased by 8 and 13 months of age, whereas the number of OPCs remained unchanged (Figures 2A–2C; Figure S2A and S2B). Previous studies have shown that APP/PS1 mice begin to display deficits in spatial memory around 8 months (Reiserer et al., 2007), and MBP protein was also decreased in the hippocampus of 8-month old APP/PS1 mice (Figure 2D), indicating a possible correlation between myelin loss and the onset of cognitive deficits. Consistently, the number of Caspr positive paranodes and MOG expression were also decreased in the cortex of 8-month-old APP/PS1 mice as compared to wildtype controls (Figures S2D and S2E). Axon densities, measured by NF200 immunostaining, were not significantly changed (Figure 2E). To confirm the loss of compact myelin, we quantified the number of myelinated axons in the corpus callosum by transmission electron microscopy. APP/PS1 mice had significantly fewer myelinated axons at 17 and 22 months of age, indicating that myelin loss occurs extensively in both gray and white matter regions (Figure 2C and S2C). To further validate that myelin degeneration is a prominent feature in AD, we examined myelin patterns in the cortex (frontal lobe) and hippocampus of AD patients and age-matched controls. MBP+ areas were significantly decreased in AD patients in both cortex and hippocampus, indicating widespread myelin loss in regions that are critical for memory and other cognitive functions (Figure 2F).

M1R deletion in OPCs enhances myelin renewal in APP/PS1 mice

The incomplete replacement of myelin loss by endogenous repair mechanisms led us to hypothesize that myelin degeneration may contribute to AD-related deficits in cognition. If this were the case, then we would expect that enhancing myelin renewal may improve the performance of APP/PS1 mice in memory-related tasks. We previously identified the muscarinic receptor 1 (M1R) as a negative regulator of OPC differentiation (Mei et al., 2016). Conditional deletion of M1R from OPCs results in enhanced OPC differentiation into mature oligodendrocytes and increased myelin formation in adult and aged mice (Wang et al., 2020). To examine whether we could also increase myelin renewal to combat AD-related myelin degeneration, we crossed APP/PS1 mice with NG2-CreERT; M1R fl/fl; Tau-mGFP to simultaneously delete M1R from OPCs and monitor the rate of new myelin formation (Figure 3). Mice were treated with tamoxifen at 7–8 months, when endogenous myelin formation was already increased in APP/PS1 mice and cognitive deficits begin to manifest (Figure 3A) (Reiserer et al., 2007). M1R deletion in OPCs was confirmed by immunostaining for M1R and PDGFRα in the M1R cKO brain three months after recombination (Figure S3A). M1R expression remained undetectable in mGFP+ pre-OLs and myelinating OLs in the APP/PS1; M1R cKO brains (Figure S3B). As expected, mGFP+ areas were exclusively co-localized with MBP-positive myelin and CC1-positive mature

OLs (Figure S3C). M1R deletion from OPCs resulted in a significant increase in mGFP+ myelin sheaths in the corpus callosum, cortex, and hippocampus of APP/PS1 mice after 3 and 6 months of recombination without affecting vascular density (CD31-positive) or cerebral blood perfusion (CBP) (Figures 3B–D; S3D and S3E). In addition, the newly generated myelin (MBP/mGFP double positive) and mature OLs (CC1/mGFP double positive) were dramatically increased in the M1R cKO brains as compared to controls from 3 to 6 months after recombination (Figures 3E and S3C). The mGFP+ myelin co-localized with Caspr, a paranodal marker expressed by axons (Figure 3F). Thus, M1R deletion from OPCs can enhance myelin renewal in APP/PS1 mice.

To evaluate the longitudinal effects of M1R deletion on myelination, we analyzed the APP/PS1; NG2-CreERT; M1R fl/fl; Tau-mGFP mice that were treated with tamoxifen at 7–8 months after three, six, or nine months (Figure S4A). mGFP+ myelin sheaths were increased by two- and three-fold in mice perfused after six and nine months, respectively, relative to mice perfused after three months (Figures S4B). Thus, M1R deletion in OPCs resulted in a stable, time-dependent increase in new myelin formation in APP/PS1 mice. Importantly, overall levels of MBP and CC1-positive cells were increased in the cortex of APP/PS1; M1R cKO cortex 6 months after recombination as compared to age-matched APP/PS1 controls (Figure 3F), suggesting that enhanced myelin renewal by M1R deletion alleviates AD-related myelin loss in the APP/PS1 mice.

Enhancing myelin renewal improves the performance of APP/PS1 mice in memory-related tasks

Recent studies have demonstrated a requirement for new myelin formation in multiple forms of learning and memory (McKenzie et al., 2014; Pan et al., 2020; Steadman et al., 2020; Wang et al., 2020; Xin and Chan, 2020), and enhancing myelination in aged mice improves their performance in a spatial memory task (Wang et al., 2020). To determine whether enhancing myelin renewal can improve cognition in AD, we trained APP/PS1 and M1R cKO; APP/PS1 mice to locate a hidden platform in an opaque water maze (Figure 4A). Over four days of training, both groups required progressively less time to reach the platform, reflecting a similar degree of spatial learning. However, during the probe test – in which the hidden platform is removed – M1R cKO; APP/PS1 made significantly more crossings into the quadrant that previously contained the platform relative to APP/PS1 mice, indicating better spatial memory (Figure 4B). This result does not seem to reflect a general increase in locomotor activity, as M1R cKO; APP/PS1 and age-matched APP/PS1 mice exhibited similar levels of activity in the open field test (Figure S5A). Furthermore, during the reversal water maze task, in which mice are trained to find the platform in a different quadrant, the M1R cKO; APP/PS1 mice again crossed more into and spent more time in the target quadrant than APP/PS1 controls, with a comparable swimming speed (Figures 4C and S5B). Interestingly, age-matched M1R cKO (without APP/PS1 mutant) and wildtype mice did not display significantly changes in the water maze task or in the open field test (Figures 4E and S5C). These results indicate that enhancing myelin renewal can improve spatial memory retention specifically in APP/PS1 mice.

To examine whether enhanced myelin renewal can benefit other types of memory tasks, M1R cKO; APP/PS1 and APP/PS1 mice were tested in the novel object recognition task (Figure 4D). Mice were placed in an arena containing two identical objects for ten minutes; two hours later, mice were reintroduced to the arena, but with one of the objects replaced by a novel object. M1R cKO; APP/PS1 mice exhibited a stronger preference for exploring the novel object, indicating better memory of the object they had previously explored (Figure 4D). Thus, enhancing myelin renewal can improve the performance of APP/PS1 mice in multiple types of memory-related tasks.

Enhancing myelin renewal increases task-related hippocampal neuronal activity in APP/PS1 mice

Previous work has shown that preventing new myelin formation impairs – and increasing new myelin formation enhances – neuronal activation induced by memory recall (Pan et al., 2020). To assess neuronal activity in APP/PS1 mice following behavior, we perfused animals trained in the water maze task within two hours after the probe test and immunostained for Fos, an immediate early gene that is upregulated in recently active neurons. The number of Fos-positive neurons was significantly increased in the hippocampus and cortex of M1R cKO; APP/PS1 mice relative to APP/PS1 controls (Figures 4F–H), whereas Fos-positive cell density was unaltered in M1R cKO mouse brains as compared to the wildtype controls (Figure S5F). These results indicate that enhancing myelin renewal can improve the reactivation of spatial memory-related neurons in APP/PS1 mice (Figures 4F–H).

Hippocampal sharp wave ripples (SPW-Rs), which occur during ‘off-line’ states like sleep, are thought to represent the compressed replay of hippocampal neuronal sequences that encode recently acquired information (Buzsáki, 2015). These replay events are critical for spatial memory consolidation (Buzsáki, 2015; Joo and Frank, 2018) but are significantly reduced in APP/PS1 mice (Cayzac et al., 2015; Jones et al., 2019). A previous study found that preventing new myelin formation disrupted the pattern of SPW-Rs that occurred following spatial learning (Steadman et al., 2020). To investigate whether SPW-Rs in APP/PS1 mice may be affected by myelin renewal, we performed multi-unit recordings in the hippocampus during sleep (Figure 5A). M1R deletion did not change the proportions of time spent in slow wave sleep, non-REM sleep, and wakefulness in APP/PS1 mice (Figure S5E). As expected, the hippocampal SPW-Rs and their peak frequency were significantly decreased in the APP/PS1 mice as compared to wildtype control (Figures 5B–D). However, both the number of hippocampal SPW-Rs and their peak frequency were significantly increased in M1R cKO; APP/PS1 mice relative to APP/PS1 mice (Figures 5B–D). Thus, enhancing myelin renewal may improve the consolidation of spatial memory by altering hippocampal replay during sleep.

Clemastine treatment rescues cognitive declines in APP/PS1 mice

Given the therapeutic implications of these results, we decided to investigate whether a pro-myelinating drug could also improve cognition in APP/PS1 mice. Clemastine fumarate has previously been used in animal models to enhance remyelination following a demyelinating injury (Mei et al., 2016), and has also been shown to enhance memory retention in aged

mice (Wang et al., 2020). Furthermore, clemastine is FDA-approved and has met clinically defined efficacy endpoints in a clinical trial in patients with chronic demyelinating injury (Green et al., 2017). We treated 8-month old APP/PS1 mice with clemastine daily for 3 months (Figure 6A). As expected, clemastine treatment resulted in a significant increase in mGFP+ new myelin in the APP/PS1; NG2-CreErt; Tau-mGFP mice as compared to the vehicle group (Figure 6B). The mice were then tested in the water maze and novel object recognition tasks. Consistent with the results from M1R cKO; APP/PS1 mice, APP/PS1 mice that received clemastine spent more time in the target quadrant and displayed a higher object recognition index relative to vehicle animals in the water maze and novel object recognition tasks, respectively (Figure 6C,E). Performance in the open field test was not significantly altered by clemastine (Figure 6D). By contrast, wildtype mice that were treated with clemastine did not display significant changes in the memory-related tasks and open field test as compared to age-matched vehicle controls (Figures 6F and S5D). Furthermore, hippocampal SPW-Rs and their peak frequency were significantly increased in APP/PS1 mice treated with clemastine as compared to the vehicle group (Figure 6G,H). Thus, systemic treatment with a pro-myelinating drug can improve memory-related task performance in APP/PS1 mice.

Enhancing myelin renewal by M1R deletion or clemastine treatment does not alter Aβ deposition or clearance

Though we showed that M1R deletion from OPCs or clemastine treatment caused a significant increase in the rate of myelin renewal, it is possible that other aspects of APP/PS1 pathology were also altered upon M1R deletion or clemastine treatment. If so, these secondary effects may be responsible for the enhanced performance of APP/PS1 in memory tasks. We examined Aβ plaques, microglial density, and microglial phagocytosis of myelin debris in M1R cKO; APP/PS1 mice. Taking into account the potential sexual dimorphism of Aβ deposition, we calculated the number of Aβ plaques in different brain regions of male and female APP/PS1 mice separately. Our results indicated that the load of Aβ plaques was not significantly changed in either male or female M1R cKO; APP/PS1 mice as compared to the sex-matched APP/PS1 controls (Figure 7A). The percentage of microglial corralling around individual Aβ plaques was not significantly altered either, as revealed by quantifying the coverage of Iba1-positive (Iba1+) cells on individual plaques (Figure 7B). To determine if the phagocytic ability of microglia was changed upon M1R deletion in OPCs, we calculated the number of Iba1+ microglia, as well as the number of microglia with internalized MBP debris (Figure 7C,D). Neither the cell densities of Iba1+ cells or the number of microglia with internalized MBP was changed upon M1R deletion in OPCs (Figure 7C,D). In line with these findings, clemastine treatment did not change the number of Aβ plaques in different brain regions of either male or female APP/PS1 brains as compared to vehicle controls (Figures 7E). Therefore, the behavioral improvement in the APP/PS1 mice with M1R cKO or clemastine treatment does not appear to result from reduced Aβ deposition or gross alterations in microglial physiology.

DISCUSSION

Cognitive impairment represents a major obstacle to daily activities for AD patients, but no disease-modifying treatments are currently available (Long and Holtzman, 2019; Scheltens et al., 2016). Multiple lines of clinical evidence have identified white matter abnormalities in AD patients (Behrendt et al., 2013; Migliaccio et al., 2012; Moghekar et al., 2012; Roseborough et al., 2017). Our results demonstrate the existence of widespread myelin loss in both AD patients and APP/PS1 mice, despite elevated endogenous levels of myelin renewal. Since demyelination disrupts neuronal conduction, and chronic demyelination results in neuronal degeneration in multiple sclerosis (MS) (Lubetzki et al., 2020), it is plausible that the extensive myelin degeneration we observed could contribute to AD-related deficits in neuronal physiology and cognitive function. In support of this hypothesis, we found that genetically or pharmacologically enhancing myelin renewal can improve the performance of APP/PS1 in memory-related tasks.

It is currently unclear why myelin loss is occurring at higher rates in APP/PS1 mice and AD patients. Though Aβ deposits can induce focal demyelination, it is worth noting that myelin loss also seemed to occur in areas devoid of Aβ deposits. Given the expression of Aβ by numerous cell types in CNS, including neurons and mature OLs (Skaper et al., 2009; Walter et al., 2019), one possible explanation is that soluble Aβ or Aβ expression in OLs may damage myelin internodes in the CNS, in which case demyelination could precede Aβ plaque formation (You et al., 2019). Consistent with this hypothesis, Aβ containing structures were initially identified in the peri-axonal space prior to any detectable Aβ plaque in white matter of 5×FAD transgenic mouse spinal cords (Chu et al., 2017). Another potential explanation for the demyelination might be an indirect response to disrupted neuronal activity; indeed, neuronal network hyperexcitability has been reported in AD brains (Cheng et al., 2020).

OPCs are widely distributed in the adult CNS and maintain their ability to proliferate and differentiate into mature oligodendrocytes. Adult OPCs maintain a constant density based on homeostatic regulation and respond robustly to myelin loss by increasing proliferation and differentiation (Hughes et al., 2013). This can be observed in preclinical mouse models for demyelinating diseases as well as in neurodegenerative disorders. For example, the rate of proliferation for OPCs is significantly increased in the SOD1 mutant mouse model for ALS, but newly differentiated oligodendrocytes undergo early apoptosis and fail to provide any supportive role (Kang et al., 2013). Similarly, the proliferation of OPCs is also increased the APP/PS1mice (Behrendt et al., 2013; Ferreira et al., 2020), though in this case, our results indicate that this increase does translate to an increase in newly formed myelin. It is still unclear whether the newly generated myelin will undergo chronic degeneration like the pre-existing myelin in APP/PS1 mice. Nevertheless, our data suggest that a large proportion of the newly formed myelin can be detected for up to 9 months in APP/PS1 mice. Unexpectedly, myelin renewal within and surrounding Aβ deposits was not significantly increased as compared to areas lacking Aβ deposits, possibly due to inhibitory cues and senescent OPCs induced by Aβ deposits (Zhang et al., 2019b).

Since interventions to prevent myelin degeneration are currently unavailable (Wu et al., 2018), enhancing myelin renewal is the more viable option in the treatment of demyelinating disease. Our data suggest that enhancing myelination may also be beneficial for patients with AD. Here we enhanced myelin renewal in APP/PS1 mice by conditional deletion of M1R in OPCs (Mei et al., 2016; Wang et al., 2020; Wang et al., 2018). It is worth noting that the density of newly formed myelin sheaths increased gradually from 3 to 9 months after recombination at 8 months of age, indicating an enduring increase in the number of stably generated sheaths and a large potential for improving upon the endogenous level of repair. More importantly, the M1R cKO; APP/PS1 mice displayed significant improvements in the water maze and novel object recognition tasks. The functional improvement in AD mice seems to be unrelated to Aβ pathology, given that neither M1R deletion in OPCs nor clemastine treatment alters Aβ load in the APP/PS1 mouse model. In line with our data, another group used administration of LINGO-1 antibodies to rescue myelin impairments and found that this treatment also alleviated memory deficits in AD mice (Wu et al., 2018). These findings support the notion that enhancing myelin renewal may lessen the degree of cognitive impairment in AD (Sun et al., 2017). As a proof of concept, we found that the myelination-enhancing drug clemastine could also improve memory retention in APP/PS1 mice.

It is surprising that M1R deletion from OPCs did not significantly alter memory task performance in 7–11 months old (middle-aged) wildtype mice, given that we previously observed M1R deletion could significantly enhance memory performance in 13–18 months old (aged) wildtype mice (Wang et al., 2020). These findings, together with the results we observed in APP/PS1 mice, suggest that M1R deletion and enhanced myelin renewal may not provide a generalized enhancement of memory, but rather only improves memory performance in cases where there is insufficient endogenous myelin renewal (i.e. in aging and AD).

The mechanisms underlying the beneficial effects of enhanced myelin renewal on cognitive impairments are still unclear. It is well known that myelin can insulate axons and protect axons from degeneration in inflammatory demyelination diseases (Lee et al., 2012; Mei et al., 2016). Recent evidence suggests that myelin renewal may also alter neuronal excitability, task-related neuronal activity, and facilitate neuronal circuit formation (Pan et al., 2020; Steadman et al., 2020; Wang et al., 2018; Xin and Chan, 2020). In support of this concept, our results indicate that enhanced myelin renewal in the APP/PS1 brains can alter task-related hippocampal activity (Buzsáki, 2015; Joo and Frank, 2018). Collectively, our results suggest that enhancing myelin renewal represents a promising therapeutic approach to alleviate AD-related impairments in cognition.

STAR★METHODS

RESOURCE AVAILABILITY

Lead Contact—Further information and requests for resources and reagents should be directed to and will be fulfilled by the Lead Contact, meif@tmmu.edu.cn (F. M.)

Materials Availability—This study did not generate new unique reagents.

Data and Code Availability—This study did not generate any datasets and code.

EXPERIMENTAL MODEL AND SUBJECT DETAILS

Animals—The mT/mG mouse line (The Jackson Laboratory, Catalog # 007676) was crossed with the PLP-CreERT line (The Jackson Laboratory, Catalog # 005795) to generate the PLP-CreERT; mT/mG mice. The NG2-CreERT line (The Jackson Laboratory, Catalog # 008538) was crossed with the Tau-mGFP (The Jackson Laboratory, Catalog # 021162) line to obtain NG2-CreERT; Tau-mGFP mice. The APP/PS1 line (APPswe, PSEN1dE9, The Jackson Laboratory, Cat: 034832) was crossed with the PLP-CreERT; mT/mG mice to generate APP/PS1; PLP-CreERT; mT/mG and the PLP-CreERT; mT/mG mice, or crossed with the NG2-CreERT; Tau-mGFP line to obtain APP/PS1;NG2-CreERT; Tau-mGFP and NG2-CreERT; Tau-mGFP mice. To generate OPC specific deletion of M1R in the APP/PS1 mice, the M1R floxed line was crossed with the APP/PS1; NG2-CreERT; Tau-mGFP line to obtain APP/PS1; NG2-CreERT; Tau-mGFP; M1R fl/fl mice and NG2-CreERT; Tau-mGFP; M1R fl/fl mice. The M1R floxed line was a generous gift from Drs. Josh Lawrence and Susumu Tonegawa and was described previously(Wang et al., 2020; Wang et al., 2018). PCR analysis of toe genomic DNA was used to distinguish different genotypes of all mouse lines with the respective primers. All mice were housed in individually ventilated cage (IVC) systems in a 12 h light/dark cycle, with free access to water and food. Male and female mice were used for all experiments. Male and female APP/PS1 mice were analyzed separately when examining Abeta plaques (Figure 7) and labeled in the behavioral tests (Figures 4, 6 and S5). Sex differences were not analyzed in myelin histology, since there is no apparaent gender bias in myelin dynamics. All animals were cared for in accordance with an approved protocol from the Laboratory Animal Welfare and Ethics Committee of the Third Military Medical University.

Human brain samples—Human brain paraffin sections were obtained from the Human Brain Bank, Chinese Academy of Medical Sciences & Peking Union Medical College, Beijing, China. The study was approved by the Institutional Review Board of the Institute of Basic Medical Science, Chinese Academy of Medical Sciences (Approval Number:009–2014). All brain samples were collected according to the standardized operational protocol published by the China Human Brain Bank Consortium. Blocks were selected from the frontal lobe and hippocampus, then sections were cut at a thickness of 5μm. Information of the donors including age, gender, degree of dementia, postmortem interval, lesion areas and neuropathologic change are summarized in Table S2.

METHOD DETAILS

Administration of tamoxifen—Tamoxifen (Sigma-Aldrich, Cat: T5648) was dissolved in corn oil at a concentration of 30mg/ml. All the mice were given tamoxifen solution at a dose of 100mg/kg per day by oral gavage for four days to induce recombination.

Drug treatment—Clemastine (SelleckChem, Cat: S1847)were orally delivered at 10mg/kg/day to the 8-month-old APP/PS1 mice and wildtype mice through drinking water for 3 months continuously. Briefly, clemastine was dissolved in dimethyl sulfoxide (DMSO) at a concentration of 30mg/ml and then diluted in drinking water. One week before the

behavior test, clemastine administration was withdrawn from all mice. Both male and female mice were pooled for analysis in this study.

Brain tissue preparation—Mice were anesthetized with 1% pentobarbital and perfused with 4% cold paraformaldehyde (PFA) in 0.1M PB transcardially after an initial flush with 0.01M phosphate-buffered saline (PBS). Brains were post-fixed in 4% PFA in 0.1M PB at 4°C for 24 hours, followed by dehydration in 30% sucrose in 0.01M PBS until submerged. Brains were embedded in optimal cutting temperature (OCT) compound (Sakura Finetek USA.Inc.,4583, USA) and cut into 20-μm-thick sections coronally using a cryostat microtome (Cyrostar NX50, Thermo Fisher, USA). The slices were kept in cryoprotectant at 4°C for storage.

In vivo electrophysiology—Under isoflurane anesthesia,M1R cKO; APP/PS1,clemastine-treated APP/PS1 mice, APP/PS1control mice and age-match wildtype mice were bilaterally implanted with tungsten tetrodes(Zhang et al., 2019a). For all in vivo electrophysiological recordings, ground and reference screws were implanted in the bone above the cerebellum. The tetrodes were implanted perpendicularly to the midline at the following coordinates: AP: −1.90 mm; ML: ±1.70 mm. During surgery, the tips of the tetrodes were lowered to the neocortex area (depth: 0.60 mm). After 3–5 days of recovery, the tetrodes were moved gradually (≤70 μm/day) until they reached the CA1 pyramidal cell layer of dorsal hippocampus, characterized by the appearance of large-amplitude SPW-R when the mice were in quiet wake or sleep state(Buzsáki, 2015).

In each mouse, electrophysiological signals were continuously recorded for at least 2hr during the light phase. As recently described(Qin et al., 2018), the signals were amplified, digitized at 20 kHz using a multiplexed preamplifier (C3334, Intan technologies) connected to a signal acquisition board (RHD2000, Intan Technologies), and stored for off-line analysis. The wide-band signal was resampled to 1250 Hz and used as local field potential (LFP). At the end of the experiment, electrolytic lesions were performed by passing DC current (30 μA for 10 s) through the bottom sites of the tetrodes, and mice were sacrificed for histological analysis 2 days later. Tetrode tip locations were verified by histological examination.

SPW-R detection and modulation analysis—The hippocampal SPW-Rs were detected during slow wave sleep.LFP signals in the hippocampus and head/neck movement of the mice were used to define the transition into distinct sleep stages (i.e., slow wave sleep and rapid eye movement sleep). One channel from a tetrode with the largest amplitude of SPW-R was chosen for the detection. The LFP signal from this channel was band-pass filtered between 100 and 250 Hz (Butterworth 3rd order), and the envelope was determined by Hilbert transform. A SPW-R event was detected if the envelope exceeded a threshold of mean plus 5 s.d. for at least 20 ms(Khodagholy et al., 2017). The onset time of individual SWR events was further utilized to calculate the SPW-R-triggered raster. The averaged SPW-R-triggered raster was used to yield a peri-SPW-R time histogram. The firing phase of hippocampal units was determined by linear interpolation between the peaks and troughs of the SPW-Rs. The peak of the SPW-R oscillation was set to 0/360°. The phase profile was

only determined for the units which fired at least 50 spikes during the detected SPW-Rs. Investigators were blinded to the genotypes of mice.

Immunofluorescence staining and images acquisition—For Immunofluorescence staining, floating sections were blocked with 5% bovine serum albumin (BSA) and 0.5% Triton-X 100 for 1h at room temperature and then sequentially incubated with primary antibodies overnight at 4°C and the fluorescent-dye-conjugated secondary antibodies for 1h at room temperature. Primary antibodies include: rabbit anti-NG2 (1:500, Millipore, Cat: AB5320), rat anti-MBP (1:200, Millipore, Cat: MAB386), rabbit anti-Iba1(1:500, Wako, Cat: 019–19741), mouse anti-β-Amyloid(1–16) (1:500,Biolegend,Cat: 803007), rabbit anti-Fos (9F6)(1:100, CST, Cat: 2250), goat anti-PDGFRα(1:200, R&D, Cat:AF-1062),rabbit Anti-muscarinic acetylcholine receptor (M1R)(1:500, Sigma, Cat: M9808), mouse anti-caspr(1:100, NeuroMab, Cat: 75–001), rabbit anti-MOG(1:200, Abcam, Cat: ab32760). Appropriate Alexa Fluor-conjugated secondary antibodies include donkey anti-mouse, donkey anti-rabbit, and goat anti-rat (1:1000, Life Technologies). The nuclei were counterstained with DAPI at room temperature. Fluorescent images were captured using a confocal laser-scanning microscope (Olympus, FV 3000, Shinjuku, Tokyo) or a spinning disk confocal super resolution microscope (Olympus, SpinSR10, Shinjuku, Tokyo) or a fluorescence microscope (Zeiss, M2, Germany) with excitation wavelengths appropriate for Alexa Fluor 350(380nm), 488 (488 nm), 594 (568 nm), 647 (628 nm) or DAPI (380 nm).

Immunohistochemistry staining—Sections were deparaffinized and rehydrated followed by heat-induced antigen retrieval. After washing with PBS, sections were treated with 3% H_2O_2 for 10 min and 5% bovine serum albumin (BSA) in PBS with 0.5% Triton X-100 for 1 h at room temperature. Then sections were incubated with primary antibody: rat anti-MBP (1:200, Millipore, Cat: MAB386) at 4°C overnight and secondary antibody (1:50, Beyotime, Cat: A0192) for 1 hour at room temperature. DAB Substrate Kit (Abcam, ab64238) was used as described by the protocol, and nuclei were counterstained with hematoxylin.

Western blotting—4-month old and 8-month-old APP/PS1 mice and age-matched wildtype mice were sacrificed to remove brain tissue. Cortex and hippocampus region were separatedand lysed by Radio Immunoprecipitation Assay (RIPA)(Beyotime, Cat: P0013B). The protein concentration was determined by BCA Assay Kit (Beyotime, Cat: P0010S). 8μg of protein was mixed with sample loading buffer (Beyotime, Cat: P0015F) and heated for 5 minutes at 100°C.Subsequently, 12% Sodium dodecyl sulfate-polyacrylamide gel electrophoresis (SDS-PAGE) gels were used to separate proteins. Proteins were then transferred ontopolyvinylidene fluoride (PVDF) membranes (Millipore, Cat: ISEQ0010) in transfer buffer containing 20% methanol for 30minutes at 0.25Ain ice. Following transfer, the membranes were blocked in 5% BSA (dissolved in tris buffered saline (TBS) containing 0.1% Tween-20) for 1 hour. Then the membrane was incubated in mouse anti-MBP antibody (1:500, Millipore, Cat: MAB386) at 4°C overnight. After washing, the membranes were incubated at 37°C for 60 min with horseradish peroxidase−labeled (HRP) secondary antibody (goat anti−mouse IgG,Beyotime, Cat: A0216) at a 1:1000 dilution. Membrane was then treated with enhanced chemiluminescent (ECL)substrate (Amercham,

RPN2231V1),visualized with ChampChemi Gel imaging system (Sage Creation, Beijing, China). After stripped with Stripping Buffer (Beyotime, P0025S) for 40 minutes, membrane was incubated with GAPDH(1:1000, Beyotime, Cat: AF0006) at 4°C overnight and HRP secondary antibody (1:1000, Beyotime, Cat: A0192) incubations done at room temperature for 1 hour. Protein level were quantified with ImageJ with normalized by GAPDH.

Electron microscopy—Before removing brain tissue, animals were perfused with 0.01 M PBS followed by 1.25% glutaraldehyde, 2% paraformaldehyde in 0.1 M PB. After post-fixation for one week, brain tissues were washed by PBS, postfixed with 1% OsO4 in PB at 4°C for 2 hours, dehydrated with graded acetone series, and stained with saturated uranyl acetate. After dehydration with graded acetone series again and embedded in Epon, ultrathin sections (~ 60 nm) were cut by using an ultramicrotome (LKB-V, LKB Produkter AB, Bromma) and observed under a transmission electron microscope (HT7700, TITACHI, Japan).

Morris water maze (MWM) task—The test was conducted according to a described protocol(Vorhees and Williams, 2006). Briefly, the water maze was divided into four quadrants. In the acquisition phase, all mice were trained two times daily for 3–5 consecutive days to find the hidden platform in the third quadrant. In probe test, the platform was removed, and time spent in the platform-located quadrant, distance travelled in platform quadrant or times crossing the platform area was measured to test short-term spatial memory. All tests were performed from 12:00 to 18:00. Investigators were blinded to the genotypes and mice were handled gently to avoid stress in the experiment.

Reverse Morris water maze task—The task was conducted 48 hours after the probe test in the MWM task according to the described protocol(Vorhees and Williams, 2006; Zhao et al., 2020). Briefly, the platform was moved to the opposite quadrant in the MWM. All mice were trained four times daily for 2 days before the probe test. Investigators were blinded to the genotypes and mice.

Novel object recognition test—As described previously(Able et al., 2006; Allen et al., 2011; Bevins and Besheer, 2006), in the familiarization session, each mouse explored two identical objects for 5minutes. 2 hours later, during the test session, one of the objects was replaced by a novel one (with different shape, similar size but in the same position) and 5minutes were given to each mouse. Object exploration was recorded when the mouse sniffed or pawed the object. Any mice that preferred one of the objects in the familiarization session or failed to explore any object were excluded. The preference for novel objects was represented by the object recognition index (ORI), which was calculated as the time of exploring novel object / time of exploring both objects. Investigators were blinded to the genotypes and mice.

Open-field Test—Open field test (OFT) was used to detect locomotor activity and exploratory behavior of mice. Mice were placed in a 50 cmX 50 cm X 50 cm arena for 20 minutes individually. The arena was divided into the center region and peripheral region by the Super Maze+ system (XinRuan Information TechnologY Co., Shanghai, China). Total distance traveled was recorded to evaluate the movement ability of mice, and the time spent

in the central area was measured to detect the anxiety of mice. Investigators were blinded to the genotypes and mice.

Microglial in vivo engulfment assay—Individual microglia were scanned with z-stacks at an interval of 0.43mm by using a confocal laser-scanning microscope (Olympus, FV3000) with a 60x objective (oil, NA1.42). All the parameters were consistent throughout all experiments. 3D surface rendering of microglial images and MBP-positive puncta were created by using Imaris x64 software (Bitplane). The proportion of Iba1-positive cells with internalized MBP debris was calculated in the hippocampus.

Cerebral Blood Perfusion (CBP)—CBP was assessed using a blood perfusion imager (PeriCamPSI System, Perimed AB, Stockholm, Sweden) based on a laserspeckle contrast imaging (LSCI) technology. Briefly, the skull of the mouse was exposed by midline skin incision, and the cerebral blood flow was detected through the skull. The unit of CBP is expressed in PU (perfusion units, PU).

QUANTIFICATION AND STATISTICAL ANALYSIS

Stereology and quantification—Brain sections were collected consecutively from Bregma 1.1mm to Bregma −2.70mm in adult mice. Corpus callosum and hippocampus were included in the sections. To sample in a systematic random manner, a set of 5–8 sections were sampled from the consecutive sections of each brain. In practice, every twentieth section was systematically sampled, the first one was randomly sampled from the first 20 sections. To quantify Fos, Iba1 and NG2 positive cells, at least three representative fields (20x) were randomly acquired from cortex and hippocampus from each brain section. To quantify MBP-positive areas in APP/PS1 mice brains or AD patient brains, and mGFP positive areas in PLP-CreERT mice brains, at least three representative fields were randomly acquired from layer 1–4 of cortex, DG and CA of hippocampus from each brain section (20x). For new myelin quantification, cortex, corpus callosum and alveus or fimbria of hippocampus were examined from each brain section.

Statistical analysis—Data were analyzed using SPSS software. All values are presented as the mean ± standard error of the mean (S.E.M). For Morris Water Maze data, repeated two-way ANOVA was used for data during the acquisition phase. For the other data, one-way ANOVA followed by Bonferroni's test was used for comparison among three groups, and unpaired t-test was used for comparison among two groups. Significance was reported as $*p< 0.05$, $**p< 0.01$ or $***p< 0.001$. All statistical tests, significance analyses, number of individual experiments (n) and other relevant information for data comparison are specified in Table S1.

Supplementary Material

Refer to Web version on PubMed Central for supplementary material.

Acknowledgments:

We would like to thank Drs. J. Josh Lawrence (Texas Tech University) and Susumu Tonegawa (MIT) for the M1R floxed mice. We would like to thank Dr. Ari Green for his insights and revision of the manuscript. We would like to acknowledge The Human Brain Bank, Chinese Academy of Medical Science & Peking Union Medical College, Beijing, China for providing the human brain sections. We would like to thank Dr. Nan-Xing Huang for drafting the graphic abstract, Ms. Wen-Xia Zheng and Mr. Heng-Sheng Tao for their assistance in imaging and quantification, and Dr. Xiao-Yong Peng for his assistance in measuring cerebral blood perfusion.

Funding:

This work was supported by the Neuroscience Center, Chinese Academy of Medical Sciences, and the Chinese Human Brain Banking Consortium, the National Natural Science Foundation of China (31970916), Chongqing Education Commission Fund (CXQT19009, BIR2019001) and Chongqing Outstanding Young Investigator Fund Project (cstc2019jcyjjqx0001) to F.M., NSFC (31671117, 31921003) to LX, the National Institutes of Health/ National Institute of Neurological Disorders and Stroke [R01NS097428, R01NS095889 to JRC and F32NS116214 to WX], The Adelson Medical Research Foundation: ANDP (A130141), and the Rachleff Family Endowment to JRC.

REFERENCES

Able JA, Gudelsky GA, Vorhees CV, and Williams MT (2006). 3,4-Methylenedioxymethamphetamine in adult rats produces deficits in path integration and spatial reference memory. Biol Psychiatry 59, 1219–1226. [PubMed: 16324685]

Allen D, Bond CT, Luján R, Ballesteros-Merino C, Lin MT, Wang K, Klett N, Watanabe M, Shigemoto R, Stackman RW Jr., et al. (2011). The SK2-long isoform directs synaptic localization and function of SK2-containing channels. Nat Neurosci 14, 744–749. [PubMed: 21602822]

Alzheimer A (1911). über eigenartige Krankheitsfälle des späteren Alters. Zeitschrift für die gesamte Neurologie und Psychiatrie 4, 356.

Arranz AM, and De Strooper B (2019). The role of astroglia in Alzheimer's disease: pathophysiology and clinical implications. Lancet Neurol 18, 406–414. [PubMed: 30795987]

Bartzokis G, Cummings JL, Sultzer D, Henderson VW, Nuechterlein KH, Mintz J. (2003) White matter structural integrity in healthy aging adults and patients with Alzheimer disease: a magnetic resonance imaging study. Archives of neurology 60: 393–398. [PubMed: 12633151]

Behrendt G, Baer K, Buffo A, Curtis MA, Faull RL, Rees MI, Götz M, and Dimou L (2013). Dynamic changes in myelin aberrations and oligodendrocyte generation in chronic amyloidosis in mice and men. Glia 61, 273–286. [PubMed: 23090919]

Benitez A, Fieremans E, Jensen JH, Falangola MF, Tabesh A, Ferris SH, and Helpern JA (2014). White matter tract integrity metrics reflect the vulnerability of late-myelinating tracts in Alzheimer's disease. NeuroImage Clinical 4, 64–71. [PubMed: 24319654]

Bevins RA, and Besheer J (2006). Object recognition in rats and mice: a one-trial non-matching-to-sample learning task to study 'recognition memory'. Nat Protoc 1, 1306–1311. [PubMed: 17406415]

Brun A, and Englund E (1986). A white matter disorder in dementia of the Alzheimer type: a pathoanatomical study. Ann Neurol 19, 253–262. [PubMed: 3963770]

Buzsáki G (2015). Hippocampal sharp wave-ripple: A cognitive biomarker for episodic memory and planning. Hippocampus 25, 1073–1188. [PubMed: 26135716]

Cayzac S, Mons N, Ginguay A, Allinquant B, Jeantet Y, and Cho YH (2015). Altered hippocampal information coding and network synchrony in APP-PS1 mice. Neurobiol Aging 36, 3200–3213. [PubMed: 26391642]

Cheng A, Wang J, Ghena N, Zhao Q, Perone I, King TM, Veech RL, Gorospe M, Wan R, and Mattson MP (2020). SIRT3 Haploinsufficiency Aggravates Loss of GABAergic Interneurons and Neuronal Network Hyperexcitability in an Alzheimer's Disease Model. J Neurosci 40, 694–709. [PubMed: 31818974]

De Strooper B, and Karran E (2016). The Cellular Phase of Alzheimer's Disease. Cell 164, 603–615. [PubMed: 26871627]

Desai MK, Mastrangelo MA, Ryan DA, Sudol KL, Narrow WC, and Bowers WJ (2010). Early oligodendrocyte/myelin pathology in Alzheimer's disease mice constitutes a novel therapeutic target. Am J Pathol 177, 1422–1435. [PubMed: 20696774]

Desai MK, Sudol KL, Janelsins MC, Mastrangelo MA, Frazer ME, and Bowers WJ (2009). Triple-transgenic Alzheimer's disease mice exhibit region-specific abnormalities in brain myelination patterns prior to appearance of amyloid and tau pathology. Glia 57, 54–65. [PubMed: 18661556]

Ferreira S, Pitman KA, Wang S, Summers BS, Bye N, Young KM, and Cullen CL (2020). Amyloidosis is associated with thicker myelin and increased oligodendrogenesis in the adult mouse brain. J Neurosci Res 98, 1905–1932. [PubMed: 32557778]

Franklin RJ, and Ffrench-Constant C (2008). Remyelination in the CNS: from biology to therapy. Nat Rev Neurosci 9, 839–855. [PubMed: 18931697]

Franklin RJ, and Goldman SA (2015). Glia Disease and Repair-Remyelination. Cold Spring Harb Perspect Biol 7, a020594. [PubMed: 25986556]

Fünfschilling U, Supplie LM, Mahad D, Boretius S, Saab AS, Edgar J, Brinkmann BG, Kassmann CM, Tzvetanova ID, Möbius W, et al. (2012). Glycolytic oligodendrocytes maintain myelin and long-term axonal integrity. Nature 485, 517–521. [PubMed: 22622581]

Gordon MN, King DL, Diamond DM, Jantzen PT, Boyett KV, Hope CE, Hatcher JM, DiCarlo G, Gottschall WP, Morgan D, et al. (2001). Correlation between cognitive deficits and Abeta deposits in transgenic APP+PS1 mice. Neurobiol Aging 22, 377–385. [PubMed: 11378242]

Green AJ, Gelfand JM, Cree BA, Bevan C, Boscardin WJ, Mei F, Inman J, Arnow S, Devereux M, Abounasr A, et al. (2017). Clemastine fumarate as a remyelinating therapy for multiple sclerosis (ReBUILD): a randomised, controlled, double-blind, crossover trial. Lancet 390, 2481–2489. [PubMed: 29029896]

Grubman A, Chew G, Ouyang JF, Sun G, Choo XY, McLean C, Simmons RK, Buckberry S, Vargas-Landin DB, Poppe D, et al. (2019). A single-cell atlas of entorhinal cortex from individuals with Alzheimer's disease reveals cell-type-specific gene expression regulation. Nat Neurosci 22, 2087–2097. [PubMed: 31768052]

Heneka MT, Carson MJ, El Khoury J, Landreth GE, Brosseron F, Feinstein DL, Jacobs AH, Wyss-Coray T, Vitorica J, Ransohoff RM, et al. (2015). Neuroinflammation in Alzheimer's disease. Lancet Neurol 14, 388–405. [PubMed: 25792098]

Henstridge CM, Hyman BT, and Spires-Jones TL (2019). Beyond the neuron-cellular interactions early in Alzheimer disease pathogenesis. Nat Rev Neurosci 20, 94–108. [PubMed: 30643230]

Hill RA, Li AM, and Grutzendler J (2018). Lifelong cortical myelin plasticity and age-related degeneration in the live mammalian brain. Nat Neurosci 21, 683–695. [PubMed: 29556031]

Hughes EG, Kang SH, Fukaya M, and Bergles DE (2013). Oligodendrocyte progenitors balance growth with self-repulsion to achieve homeostasis in the adult brain. Nat Neurosci 16, 668–676. [PubMed: 23624515]

Hughes EG, Orthmann-Murphy JL, Langseth AJ, and Bergles DE (2018). Myelin remodeling through experience-dependent oligodendrogenesis in the adult somatosensory cortex. Nat Neurosci 21, 696–706. [PubMed: 29556025]

Jankowsky JL, Fadale DJ, Anderson J, Xu GM, Gonzales V, Jenkins NA, Copeland NG, Lee MK, Younkin LH, Wagner SL, et al. (2004). Mutant presenilins specifically elevate the levels of the 42 residue beta-amyloid peptide in vivo: evidence for augmentation of a 42-specific gamma secretase. Hum Mol Genet 13, 159–170. [PubMed: 14645205]

Jones EA, Gillespie AK, Yoon SY, Frank LM, and Huang Y (2019). Early Hippocampal Sharp-Wave Ripple Deficits Predict Later Learning and Memory Impairments in an Alzheimer's Disease Mouse Model. Cell Rep 29, 2123–2133.e2124. [PubMed: 31747587]

Joo HR, and Frank LM (2018). The hippocampal sharp wave-ripple in memory retrieval for immediate use and consolidation. Nat Rev Neurosci 19, 744–757. [PubMed: 30356103]

Kang SH, Li Y, Fukaya M, Lorenzini I, Cleveland DW, Ostrow LW, Rothstein JD, and Bergles DE (2013). Degeneration and impaired regeneration of gray matter oligodendrocytes in amyotrophic lateral sclerosis. Nat Neurosci 16, 571–579. [PubMed: 23542689]

Khodagholy D, Gelinas JN, and Buzsáki G (2017). Learning-enhanced coupling between ripple oscillations in association cortices and hippocampus. Science 358, 369–372. [PubMed: 29051381]

Lee Y, Morrison BM, Li Y, Lengacher S, Farah MH, Hoffman PN, Liu Y, Tsingalia A, Jin L, Zhang PW, et al. (2012). Oligodendroglia metabolically support axons and contribute to neurodegeneration. Nature 487, 443–448. [PubMed: 22801498]

Long JM, and Holtzman DM (2019). Alzheimer Disease: An Update on Pathobiology and Treatment Strategies. Cell 179, 312–339. [PubMed: 31564456]

Lubetzki C, Zalc B, Williams A, Stadelmann C, and Stankoff B (2020). Remyelination in multiple sclerosis: from basic science to clinical translation. Lancet Neurol 19, 678–688. [PubMed: 32702337]

Luo X, Li K, Zeng Q, Huang P, Jiaerken Y, Wang S, Shen Z, Xu X, Xu J, Wang C, et al. (2019). Application of T1-/T2-Weighted Ratio Mapping to Elucidate Intracortical Demyelination Process in the Alzheimer's Disease Continuum. Front Neurosci 13, 904. [PubMed: 31551678]

Mathys H, Davila-Velderrain J, Peng Z, Gao F, Mohammadi S, Young JZ, Menon M, He L, Abdurrob F, Jiang X, et al. (2019). Single-cell transcriptomic analysis of Alzheimer's disease. Nature 570, 332–337. [PubMed: 31042697]

McKenzie IA, Ohayon D, Li H, de Faria JP, Emery B, Tohyama K, and Richardson WD (2014). Motor skill learning requires active central myelination. Science 346, 318–322. [PubMed: 25324381]

Mei F, Lehmann-Horn K, Shen YA, Rankin KA, Stebbins KJ, Lorrain DS, Pekarek K, S, A.S., Xiao L, Teuscher C, et al. (2016). Accelerated remyelination during inflammatory demyelination prevents axonal loss and improves functional recovery. Elife 5.

Migliaccio R, Agosta F, Possin KL, Rabinovici GD, Miller BL, and Gorno-Tempini ML (2012). White matter atrophy in Alzheimer's disease variants. Alzheimers Dement 8, S78–87.e71–72. [PubMed: 23021625]

Mitew S, Kirkcaldie MT, Halliday GM, Shepherd CE, Vickers JC, and Dickson TC (2010). Focal demyelination in Alzheimer's disease and transgenic mouse models. Acta Neuropathol 119, 567–577. [PubMed: 20198482]

Moghekar A, Kraut M, Elkins W, Troncoso J, Zonderman AB, Resnick SM, and O'Brien RJ (2012). Cerebral white matter disease is associated with Alzheimer pathology in a prospective cohort. Alzheimers Dement 8, S71–77. [PubMed: 23021624]

Mot AI, Depp C, and Nave KA (2018). An emerging role of dysfunctional axon-oligodendrocyte coupling in neurodegenerative diseases. Dialogues Clin Neurosci 20, 283–292. [PubMed: 30936768]

Murray ME, Graff-Radford NR, Ross OA, Petersen RC, Duara R, and Dickson DW (2011). Neuropathologically defined subtypes of Alzheimer's disease with distinct clinical characteristics: a retrospective study. Lancet Neurol 10, 785–796. [PubMed: 21802369]

Pan S, Mayoral SR, Choi HS, Chan JR, and Kheirbek MA (2020). Preservation of a remote fear memory requires new myelin formation. Nat Neurosci 23, 487–499. [PubMed: 32042175]

Phillips OR, Joshi SH, Piras F, Orfei MD, Iorio M, Narr KL, Shattuck DW, Caltagirone C, Spalletta G, and Di Paola M (2016). The superficial white matter in Alzheimer's disease. Hum Brain Mapp 37, 1321–1334. [PubMed: 26801955]

Qin H, Fu L, Hu B, Liao X, Lu J, He W, Liang S, Zhang K, Li R, Yao J, et al. (2018). A Visual-Cue-Dependent Memory Circuit for Place Navigation. Neuron 99, 47–55.e44. [PubMed: 29909996]

Reiserer RS, Harrison FE, Syverud DC, and McDonald MP (2007). Impaired spatial learning in the APPSwe + PSEN1DeltaE9 bigenic mouse model of Alzheimer's disease. Genes Brain Behav 6, 54–65. [PubMed: 17233641]

Ringman JM, O'Neill J, Geschwind D, Medina L, Apostolova LG, Rodriguez Y, Schaffer B, Varpetian A, Tseng B, Ortiz F, et al. (2007). Diffusion tensor imaging in preclinical and presymptomatic carriers of familial Alzheimer's disease mutations. Brain 130, 1767–1776. [PubMed: 17522104]

Roseborough A, Ramirez J, Black SE, and Edwards JD (2017). Associations between amyloid β and white matter hyperintensities: A systematic review. Alzheimers Dement 13, 1154–1167. [PubMed: 28322203]

Scheltens P, Blennow K, Breteler MM, de Strooper B, Frisoni GB, Salloway S, and Van der Flier WM (2016). Alzheimer's disease. Lancet 388, 505–517. [PubMed: 26921134]

Schmued LC, Raymick J, Paule MG, Dumas M, and Sarkar S (2013). Characterization of myelin pathology in the hippocampal complex of a transgenic mouse model of Alzheimer's disease. Current Alzheimer research 10, 30–37. [PubMed: 23157338]

Skaper SD, Evans NA, Evans NA, Rosin C, Facci L, and Richardson JC (2009). Oligodendrocytes are a novel source of amyloid peptide generation. Neurochem Res 34, 2243–2250. [PubMed: 19557514]

Steadman PE, Xia F, Ahmed M, Mocle AJ, Penning ARA, Geraghty AC, Steenland HW, Monje M, Josselyn SA, and Frankland PW (2020). Disruption of Oligodendrogenesis Impairs Memory Consolidation in Adult Mice. Neuron 105, 150–164.e156. [PubMed: 31753579]

Stricker NH, Schweinsburg BC, Delano-Wood L, Wierenga CE, Bangen KJ, Haaland KY, Frank LR, Salmon DP, and Bondi MW (2009). Decreased white matter integrity in late-myelinating fiber pathways in Alzheimer's disease supports retrogenesis. Neuroimage 45, 10–16. [PubMed: 19100839]

Sun J, Zhou H, Bai F, Zhang Z, and Ren Q (2017). Remyelination: A Potential Therapeutic Strategy for Alzheimer's Disease? J Alzheimers Dis 58, 597–612. [PubMed: 28453483]

Taylor ANW, Kambeitz-Ilankovic L, Gesierich B, Simon-Vermot L, Franzmeier N, Araque Caballero M, Müller S, Hesheng L, Ertl-Wagner B, Bürger K, et al. (2017). Tract-specific white matter hyperintensities disrupt neural network function in Alzheimer's disease. Alzheimers Dement 13, 225–235. [PubMed: 27432800]

Vorhees CV, and Williams MT (2006). Morris water maze: procedures for assessing spatial and related forms of learning and memory. Nat Protoc 1, 848–858. [PubMed: 17406317]

Walter S, Jumpertz T, Hüttenrauch M, Ogorek I, Gerber H, Storck SE, Zampar S, Dimitrov M, Lehmann S, Lepka K, et al. (2019). The metalloprotease ADAMTS4 generates N-truncated Aβ4-x species and marks oligodendrocytes as a source of amyloidogenic peptides in Alzheimer's disease. Acta Neuropathol 137, 239–257. [PubMed: 30426203]

Wang C, Xiong M, Gratuze M, Bao X, Shi Y, Andhey PS, Manis M, Schroeder C, Yin Z, Madore C, et al. (2021). Selective removal of astrocytic APOE4 strongly protects against tau-mediated neurodegeneration and decreases synaptic phagocytosis by microglia. Neuron

Wang F, Ren SY, Chen JF, Liu K, Li RX, Li ZF, Hu B, Niu JQ, Xiao L, Chan JR, et al. (2020). Myelin degeneration and diminished myelin renewal contribute to age-related deficits in memory. Nat Neurosci 23, 481–486. [PubMed: 32042174]

Wang F, Yang YJ, Yang N, Chen XJ, Huang NX, Zhang J, Wu Y, Liu Z, Gao X, Li T, et al. (2018). Enhancing Oligodendrocyte Myelination Rescues Synaptic Loss and Improves Functional Recovery after Chronic Hypoxia. Neuron 99, 689–701.e685. [PubMed: 30078577]

Wu D, Tang X, Gu LH, Li XL, Qi XY, Bai F, Chen XC, Wang JZ, Ren QG, and Zhang ZJ (2018). LINGO-1 antibody ameliorates myelin impairment and spatial memory deficits in the early stage of 5XFAD mice. CNS Neurosci Ther 24, 381–393. [PubMed: 29427384]

Xin W, and Chan JR (2020). Myelin plasticity: sculpting circuits in learning and memory. Nat Rev Neurosci

You Y, Joseph C, Wang C, Gupta V, Liu S, Yiannikas C, Chua BE, Chitranshi N, Shen T, Dheer Y, et al. (2019). Demyelination precedes axonal loss in the transneuronal spread of human neurodegenerative disease. Brain 142, 426–442. [PubMed: 30668642]

Young KM, Psachoulia K, Tripathi RB, Dunn SJ, Cossell L, Attwell D, Tohyama K, and Richardson WD (2013). Oligodendrocyte dynamics in the healthy adult CNS: evidence for myelin remodeling. Neuron 77, 873–885. [PubMed: 23473318]

Zhang J, Zhang KY, Zhang LB, Zhang WW, Feng H, Yao ZX, Hu B, and Chen H (2019a). A method for combining multiple-units readout of optogenetic control with natural stimulation-evoked eyeblink conditioning in freely-moving mice. Sci Rep 9, 1857. [PubMed: 30755637]

Zhang P, Kishimoto Y, Grammatikakis I, Gottimukkala K, Cutler RG, Zhang S, Abdelmohsen K, Bohr VA, Misra Sen J, Gorospe M, et al. (2019b). Senolytic therapy alleviates Aβ-associated oligodendrocyte progenitor cell senescence and cognitive deficits in an Alzheimer's disease model. Nat Neurosci 22, 719–728. [PubMed: 30936558]

Zhao Y, Qian R, Zhang J, Liu F, Iqbal K, Dai CL, and Gong CX (2020). Young blood plasma reduces Alzheimer's disease-like brain pathologies and ameliorates cognitive impairment in 3×Tg-AD mice. Alzheimers Res Ther 12, 70. [PubMed: 32513253]

Zhou Y, Song WM, Andhey PS, Swain A, Levy T, Miller KR, Poliani PL, Cominelli M, Grover S, Gilfillan S, et al. (2020). Human and mouse single-nucleus transcriptomics reveal TREM2-dependent and TREM2-independent cellular responses in Alzheimer's disease. Nat Med 26, 131–142. [PubMed: 31932797]

Highlights:

- Myelination is increased in APP/PS1 mice in responding to demyelination.
- Extensive myelin loss occurs in APP/PS1 mice brains and postmortem AD tissue.
- Pro-myelinating strategies enhances myelin renewal and alleviates myelin loss.
- Enhanced myelin renewal rescues AD-related deficits in cognition and SWRs.

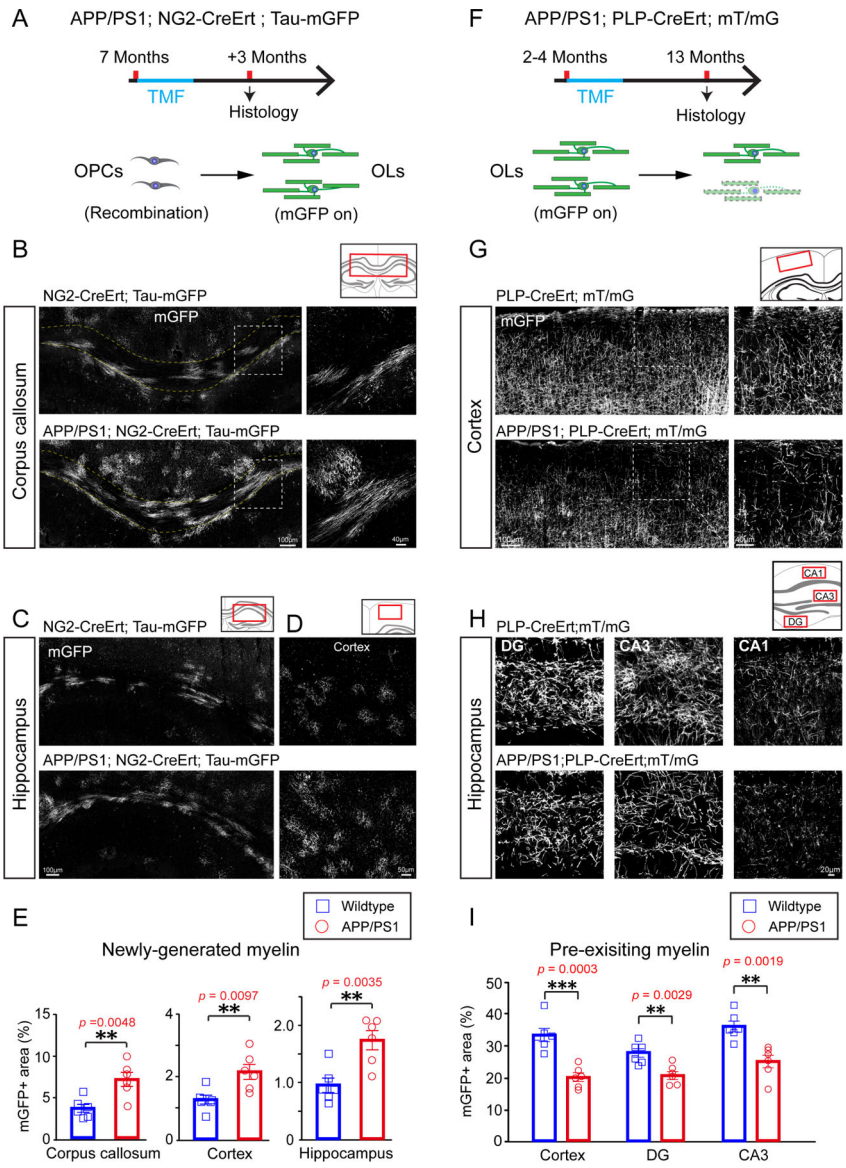

Figure 1. New myelin formation and degeneration are both elevated in APP/PS1 mice.

(A) Schematic illustration showing the time course for tamoxifen induction and histology in the APP/PS1;NG2-CreERT;Tau-mGFP mice. **(B-D)** Confocal images of mGFP positive myelin (gray) in the corpus callosum **(B)**, hippocampus **(C)** and cortex **(D)** of APP/PS1 mice and littermate controls. Magnified images (right panels) showing the dotted areas in the left panels in **B**. Scale bars, 100μm (left panels of **B, C**), 40μm (right panels of **B**) and 50μm **(D)**. **(E)** Quantification of mGFP positive myelin in the corpus callosum, hippocampus and cortex of APP/PS1 mice and littermate controls. n=6 biologically independent mice for each group, two-tailed unpaired *t*-tests were used; **(F)** Schematic illustration displaying the time course for tamoxifen induction and histology in the APP/PS1;PLP-CreERT;mT/mG mice.**(G and H)**Representative images of mGFP positive myelin (gray) in the cortex **(G)**and hippocampus **(H)** of APP/PS1 mice and littermate controls. Scale bars, 100μm (left panels of **G**), 40μm (right panels of **G**), 20μm (**H**). **(I)** Quantification of mGFP positive myelin areas

in the cortex and hippocampus of APP/PS1 mice and littermate controls. n=6 biologically independent mice for each group, two-tailed unpaired *t*-tests were used; Error bars are presented as mean ± s.e.m. *$p<0.05$, **$p<0.01$, ***$p<0.001$. See also Figure S1 and Table S1.

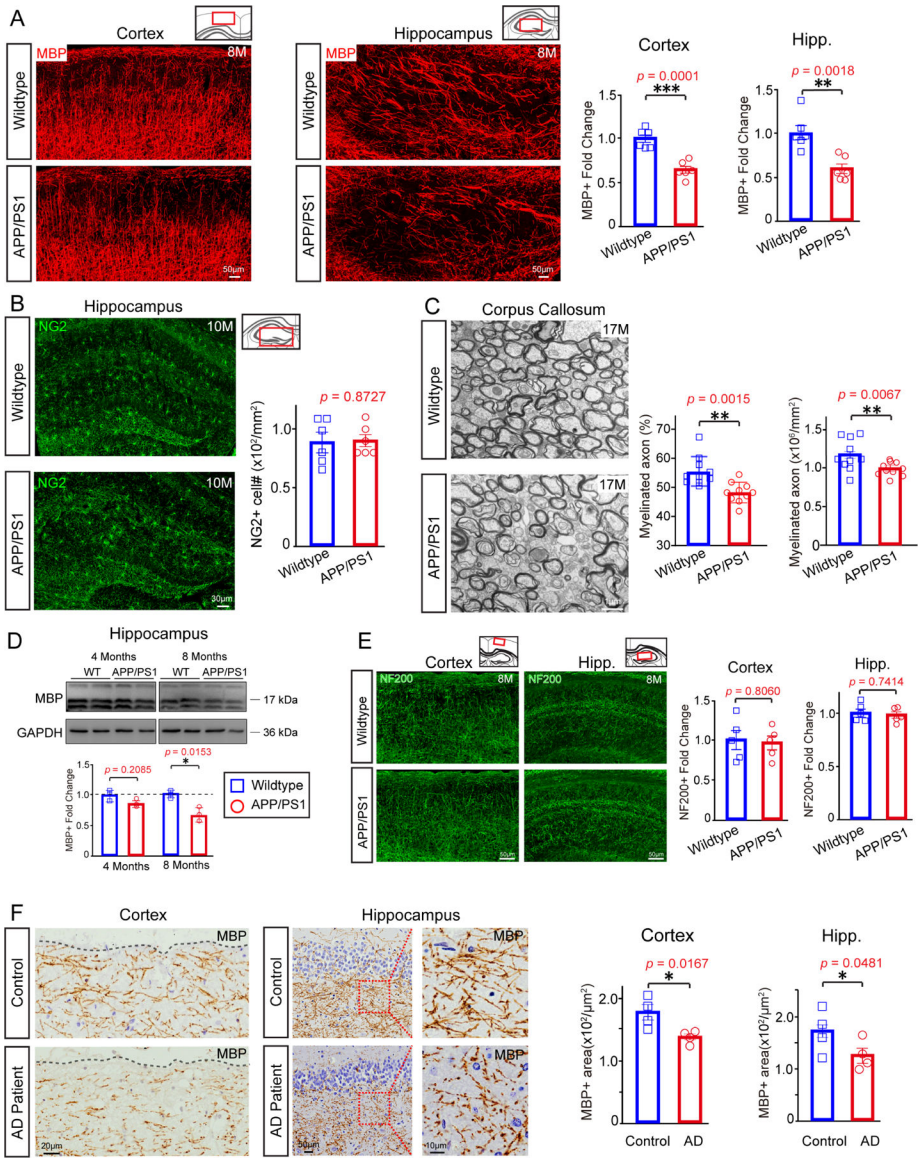

Figure 2. Extensive myelin loss in APP/PS1 mice and individuals with AD.

(A) Representative images and quantification of fold change of MBP-positive areas in cortex and hippocampus of 8-month old APP/PS1 transgenic mice and age-matched wildtype controls. n=6 mice in each group, significance was determined using two-tailed unpaired *t*-tests. Scale bar,50μm. **(B)** Confocal images and quantification of NG2 positive OPCs in the hippocampus of 10-month old APP/PS1 transgenic mice and controls. n=6 biologically independent mice for each group, two-tailed unpaired *t*-tests were used. Scale bar, 30μm. **(C)** Electron micrographs and quantification of myelinated axons in the corpus callosum of 17-month old APP/PS1 mice and littermate controls. Scale bar: 1μm; $n = 10$ images (2k) from 3 mice in each group. Two-tailed unpaired *t*-tests were used. **(D)** Blots show MBP of 4-month-old, 8-month-old wildtype and APP/PS1 mice brain. n=4 biologically independent mice for each group. Two-tailed unpaired *t*-tests were used. **(E)** Representative images and quantification of NF200-positive areas in cortex and hippocampus of 8-month old APP/PS1

transgenic mice and age-matched wildtype controls. n=5 mice in each group, significance was determined using two-tailed unpaired *t*-tests. Scale bar,50μm. **(F)** Representative images and quantification of MBP positive areas in the frontal lobe (left panels) and hippocampus (right and middle panels) of AD patients and age-matched controls. The right panels display magnified images corresponding to the dotted boxes in the middle panels. n=4 biologically independent patients for each group. Two-tailed unpaired *t*-tests were used. Scale bars, 20μm (left panels), 50μm (middle panels), 10μm (right panels). Error bars are presented as mean ± s.e.m. *$p<0.05$, **$p<0.01$, ***$p<0.001$. See also Figure S2 and Table S1.

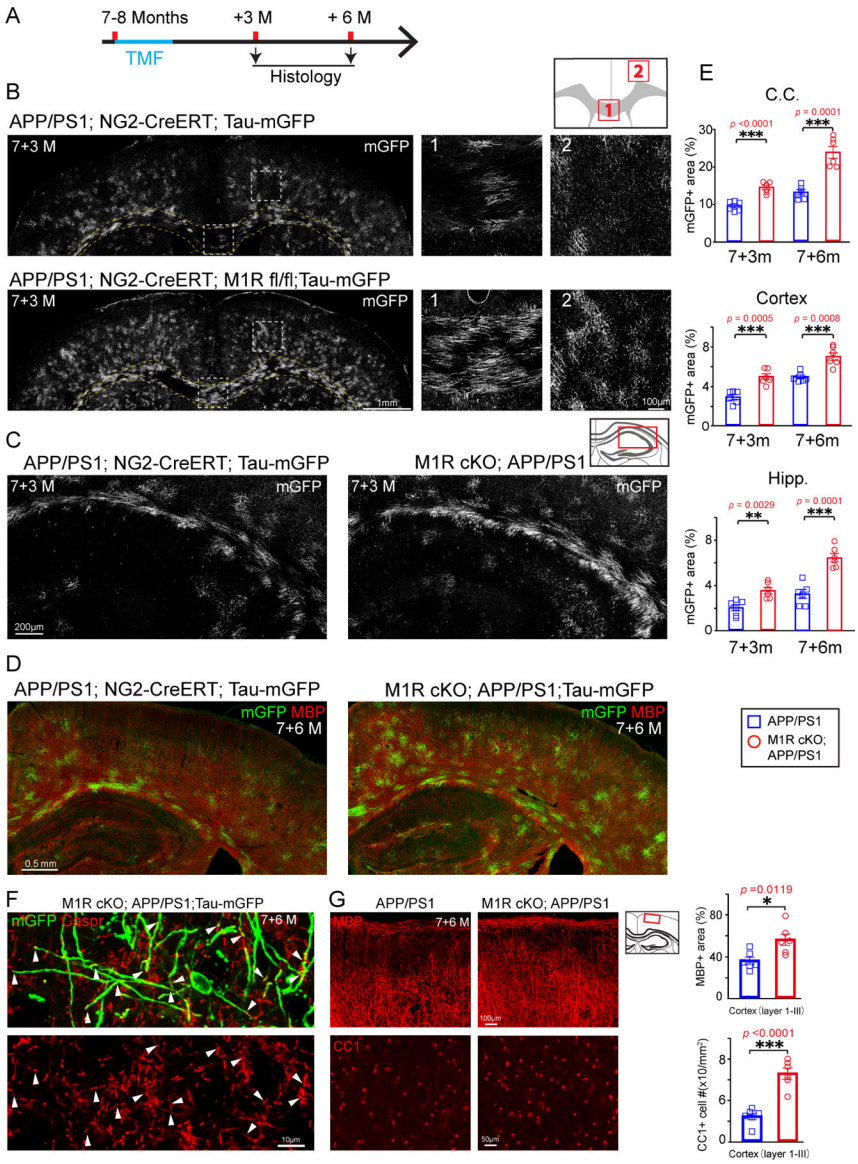

Figure 3. M1R deletion in OPCs enhances myelin renewal and alleviates myelin loss.

(A) Schematic illustration displaying the time course for tamoxifen induction and histology of the APP/PS1;NG2-CreERT;Tau-mGFP (APP/PS1) and APP/PS1; NG2-CreERT; Tau-mGFP; M1R fl/fl (M1R cKO; APP/PS1) mice. **(B and C)** Representative images of mGFP positive myelin (gray) in the corpus callosum **(B, B1)**, cortex **(B, B2)** and hippocampus **(C)** of 7+3m APP/PS1; M1R cKO and APP/PS1 mice. Magnified images **(B1, B2)** corresponding to the dotted boxes in the left panels (**B**). Scale bars, 1mm (left panels of **B**),100μm **(B1 and B2)**, 200μm **(C). (D)** Representative images of mGFP (green) and MBP (red) positive myelin in the APP/PS1; M1R cKO and APP/PS1 mice. Scale bars, 0.5mm**. (E)** Quantification of mGFP positive myelin in the corpus callosum, cortex and hippocampus in APP/PS1 M1R cKO and APP/PS1 mice. n=6 biologically independent mice for each group, two-tailed unpaired *t*-tests were used.**(F)**Confocal images showing Caspr positive paranodes (arrowheads) in mGFP positive myelin. Scale bars, 10μm. **(G)** Confocal images and

quantification of CC1 positive mature OLs (lower two panels) and MBP positive myelin (upper two panels) in the cortex of 7+6-month-old APP/PS1; M1R cKO and APP/PS1 mice. Scale bars, 100μm (upper panels), 50μm (lower panels). n=6 biologically independent mice for each group. Error bars are presented as mean ± s.e.m. *p<0.05, **p<0.01, ***p<0.001. See also Figure S3 and Table S1.

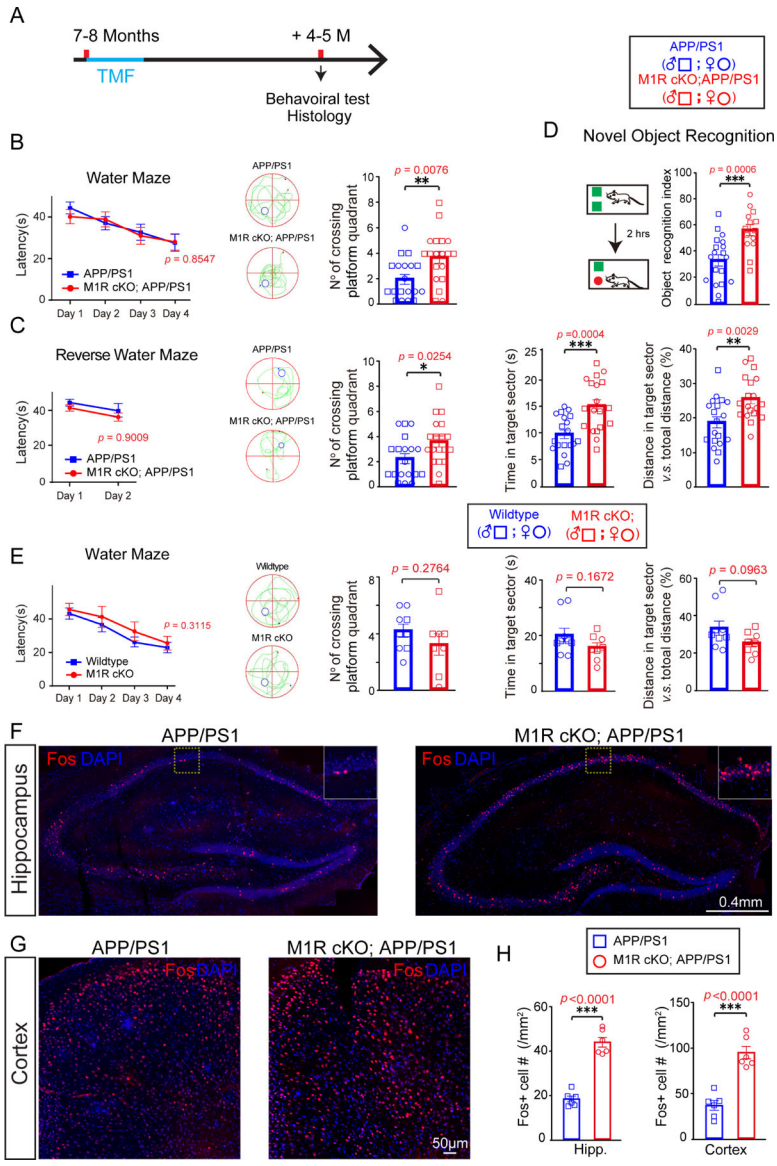

Figure 4. Improved performances of memory-related tasks in APP/PS1; M1R cKO mice.

(A) Schematic diagram displaying the time course for tamoxifen induction, behavioral test and histology. **(B)** Graphs showing latencies to platform in acquisition phase and number of platform crossings in probing for the Morris water maze task with the APP/PS1 mice. Two-way repeat ANOVA was used for the latency to platform; two-tailed unpaired *t*-tests were used for number of platform crossings. **(C)** Reverse water maze task revealing latencies to platform in acquisition phase, numbers of platform crossings, and time and distance spent in the target quadrant. Two-way repeat ANOVA was used for the latency to platform; two-tailed unpaired *t*-tests were used for number of platform crossings, time, and distance spent in the target quadrant. **(D)** Graph showing novel object recognition index of APP/PS1 mice and M1R cKO; APP/PS1 mice. Two-tailed unpaired *t*-tests was used. **(E)** Water maze test revealed the latency to platform in the acquisition phase, their number of crossing platform quadrant, time in target sector and the distance in target sector of wildtype and M1R cKO

mice. Two-way repeat ANOVA was used for the latency to platform; two-tailed unpaired t-tests were used for number of platform crossings, time in target sector and the distance in target sector. **(F-H)** Representative images and quantification of Fos+ (red) cells in the hippocampus **(F, H)** and cortex **(G, H)** of APP/PS1 and M1R cKO; APP/PS1 mice. Scale bar, 0.4 mm **(F)**, 50**μ**m **(G)**. Two-tailed unpaired *t*-tests were used. Data points represents individual animals. Error bars are presented as mean ± s.e.m. *$p<0.05$, **$p<0.01$, ***$p<0.001$. See also Figures S5 and Table S1.

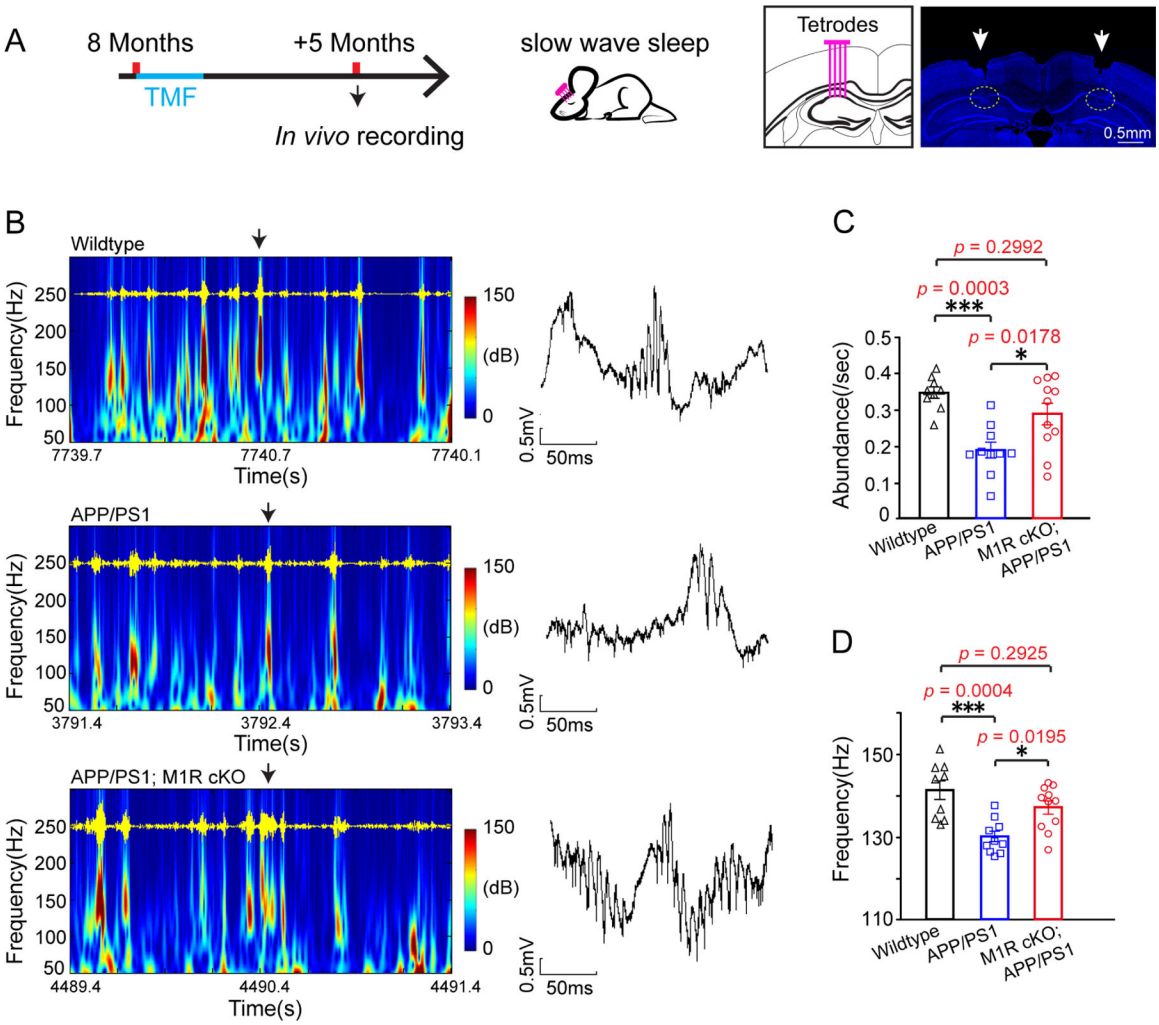

Figure 5. M1R deletion changes hippocampal SPW-Rs and firing activity of hippocampal pyramidal cells in APP/PS1 mice.

(A) Schematic diagram displaying the time course for tamoxifen induction and *in vivo* recordings. Representative images showing the location of tetrode implantation. Scale bar, 0.5mm. **(B)** Hippocampal local field potential (LFP) spectra from the wildtype, APP/PS1 and M1R cKO; APP/PS1 mice. SPW-R oscillations (100–250 Hz) are illustrated and highlighted in red. Representative LFP traces indicated by black arrows illustrates SPW-Rs in the right panel. Scale bars: 0.5 mV, 50 ms; **(C and D)** Quantification of SPW-R abundance **(C)** and SPW-R peak frequency **(D)** in the wildtype (n = 9 sessions from 3 mice, gray squares), APP/PS1 mice (n=10 sessions from 3 mice, blue squares) and M1R cKO; APP/PS1 (n = 11 sessions from 3 mice, red circles). Two-tailed unpaired *t*-tests were used. Error bars are presented as mean ± s.e.m. *p<0.05, **p<0.01, ***p<0.001. See also Figure S5 and Table S1.

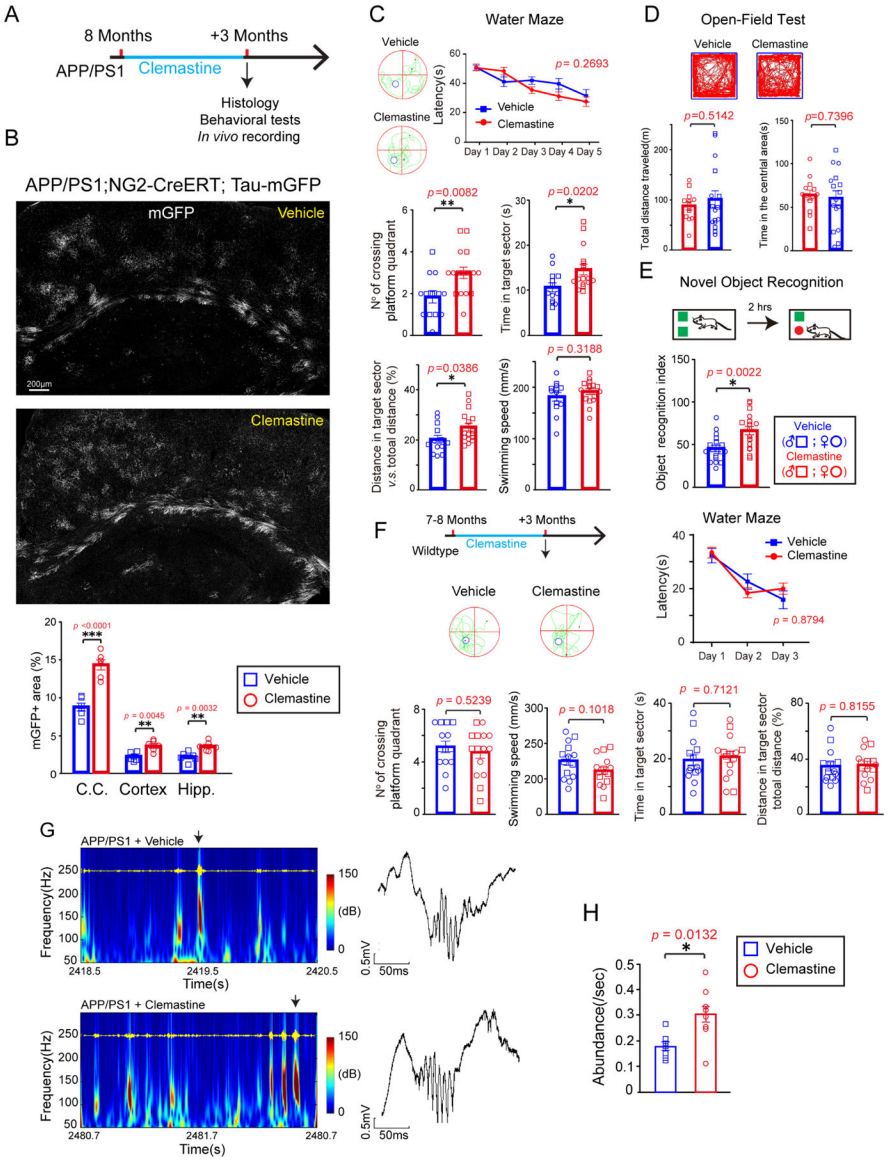

Figure 6. Clemastine treatment rescues cognitive declines in APP/PS1 mice.

(A) Schematic diagram displaying the time course for clemastine treatment, behavior test, *in vivo* recording and histology. **(B)** Representative images and quantification of mGFP positive myelin (grey) in the brain of APP/PS1; NG2-CreErt; Tau-mGFP mice induced with tamoxifen and treated with clemastine for 3 months. Two-tailed unpaired *t*-tests were used. Scale bar, 200μm. **(C)** Graphs showing latencies to platform in acquisition phase, the number of platform crossings, time and distance spent in target quadrant, swimming speed in probe test in the Morris water maze task of APP/PS1 mice after a 3-monthtreatment of clemastine or vehicle. Two-way repeat ANOVA was used for the latency to platform; two-tailed unpaired *t*-tests were used for number of platform crossings, time, swimming speed and distance spent in the target quadrant. See Table S1 for the statistical details. **(D)** Graphs showing total distance and time in the central area in the open field test. **(E)** Graph showing novel object recognition index of APP/PS1 mice treated with or without clemastine; Two-

tailed unpaired *t*-tests was used. **(F)** Water maze test revealed the latency to platform in the acquisition phase, the number of crossing platform quadrant, time in target sector and the distance in target sector of wildtype mice treated with or without clemastine. Two-way repeat ANOVA was used for the latency to platform; two-tailed unpaired t-tests were used for number of platform crossings, time in target sector and the distance in target sector. **(G)** Hippocampal local field potential (LFP) spectra from the vehicle and clemastine treated APP/PS1 mice. SPW-R oscillations (100–250 Hz) are illustrated and highlighted in red. Representative LFP traces indicated by black arrows illustrates SPW-Rs in the right panel. Scale bars: 0.5 mV, 50 ms; **(H)** Quantification of SPW-R abundance in the vehicle (n = 7 sessions from 3 mice), clemastine treatment (n=8 sessions from 3 mice). Two-tailed unpaired *t*-tests were used. Error bars are presented as mean ± s.e.m. *p<0.05, **p <0.01, ***p<0.001. See also Figure S5 and Table S1.

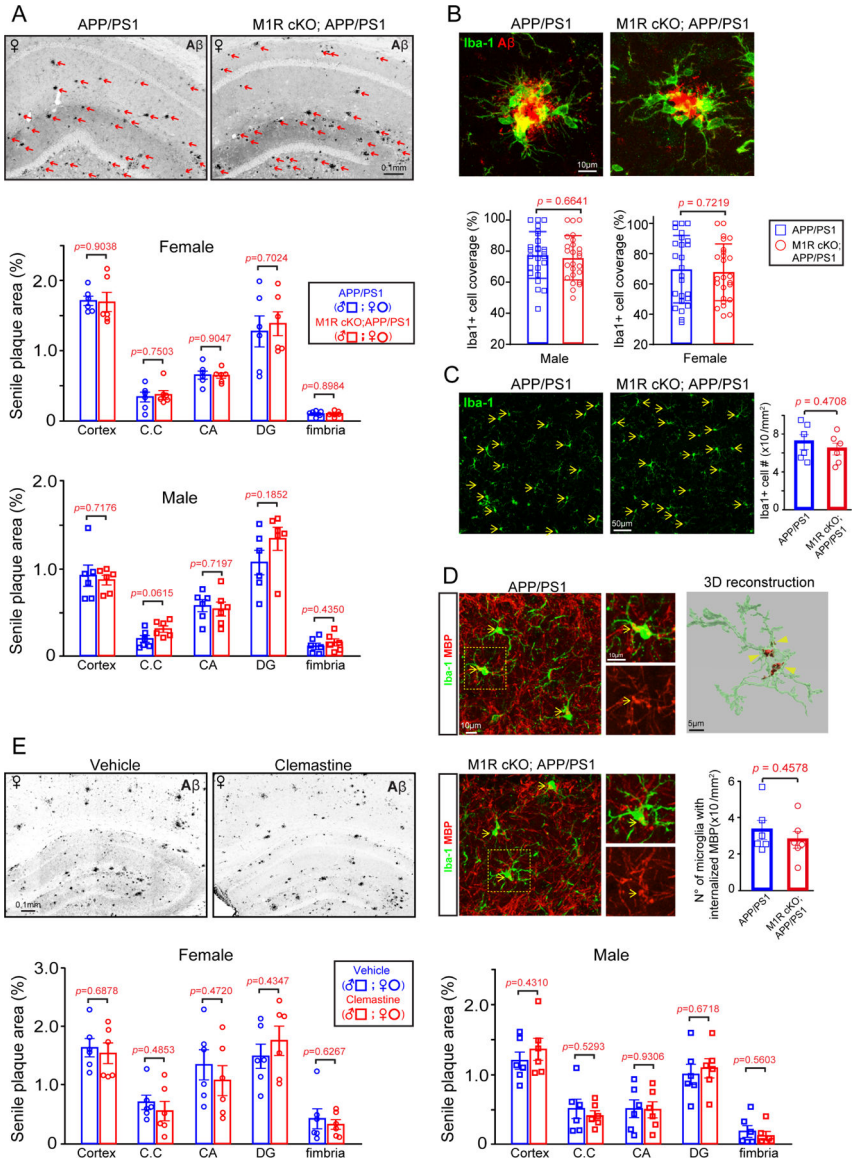

Figure 7. OPC-specific M1R deletion and clemastine treatment does not alter Aβ deposition or clearance in APP/PS1 mice.

(A) Representative images and quantification of Aβ plaques (red arrows) in different brain regions of male or female APP/PS1 and APP/PS1; M1R cKO mice; scale bar = 0.1mm. n=6 mice for each group; **(B)** Micrographs showing Aβ plaques (red) and associated Iba+ cells (green) and quantification of the corralling percentage of Iba1+ cells around individual Aβ plaques in male or female APP/PS1 and APP/PS1; M1R cKO mouse brains; scale bar = 10μm. n=6 mice for each group; **(C)** Representative images and quantification of Iba1+ cell density in APP/PS1 and APP/PS1; M1R cKO cortex; scale bar = 50μm. n=6 mice for each group; **(D)** Representative images and quantification of engulfed myelin debris (red, arrows) by Iba1+ microglia in APP/PS1 and APP/PS1; M1R cKO cortex; scale bar = 10μm. Enlarged images (right panels) correspond to the dotted boxes in the left panels. 3D reconstruction of engulfed myelin debris (red, arrowheads) in an Iba1+ microglia (green); scale bar = 5μm. n=6 mice for each group. **(E)** Representative images and quantification of

Aβ plaques in different brain regions of male or female APP/PS1 mice treated with vehicle or clemastine; scale bar = 0.1mm. n=6 mice for each group. Error bars are presented as mean ± s.e.m.

KEY RESOURCES TABLE

REAGENT or RESOURCE	SOURCE	IDENTIFIER
Antibodies		
Rat anti-MBP	Millipore	Cat# MAB386 RRID:AB_94975
Rabbit anti-NG2	Millipore	Cat# AB5320 RRID:AB_11213678
Rabbit anti-Iba1	Wako	Cat# 019-19741 RRID:AB_839504
Mouse anti-β-Amyloid(1-16)	BioLegend	Cat# 803007 RRID:AB_2564657
Rabbit anti-Fos(9F6)	Cell Signaling Technology	Cat#2250 RRID:AB_2247211
Goat anti-PDGFRα	R&D	Cat#AF-1062 RRID:AB_2236897
Rabbit Anti-Muscarinic Acetylcholine Receptor(M1)	Sigma	Cat#M9808 RRID:AB_260731
Mouse anti-caspr	NeuroMab	Cat#75-001 RRID:AB_2083496
Rabbit anti-Myelin oligodendrocyte glycoprotein	Abcam	Cat# AB32760, RRID:AB_2145529
Mouse anti-CC1	Millipore	Cat#OP80 RRID:AB_2057371
Anti-NF200	Sigma	Cat#N4142 RRID:AB_477272
Goat anti-GFP	Abcam	Cat#AB5450 RRID:AB_304897
Mouse anti-GAPDH	Beyotime	Cat#AF0006
Alexa Fluor 568 donkey anti-rabbit IgG	Thermo Fisher Scientific	Cat# A-10042, RRID:AB_2534017
Alexa Fluor 594 donkey anti-rat IgG	Thermo Fisher Scientific	Cat# A-21209, RRID:AB_2535795
Alexa Fluor 488 donkey anti-rat IgG	Thermo Fisher Scientific	Cat# A-21206, RRID:AB_2535792
Alexa Fluor 350 donkey anti-mouse IgG	Thermo Fisher Scientific	Cat# A-10035, RRID:AB_2534011
Alexa Fluor 365 donkey anti-rabbit IgG	Thermo Fisher Scientific	Cat# A-31576, RRID:AB_10374303
Alexa Fluor 647 donkey anti-rat IgG	Abcam	Cat# ab150155, RRID:AB_2813835
HRP goat anti rat IgG	Beyotime	Cat#A0192
HRP goat anti mouse IgG	Beyotime	Cat#A0216
Biological Samples		
Human brain sections	Human Brain Bank, Chinese Academy of Medical Sciences & Peking Union Medical College. (Refer to Table S2 for detailed information)	N/A
Chemicals, Peptides, and Recombinant Proteins		
Tamoxifen	Sigma-Aldrich	Cat# T5648
Clemastine	SelleckChem	Cat# S1847
RIPA Lysis Buffer	Beyotime,Shanghai	Cat# P0013B
Tissue-Tek OCT compound	Sakura	4583
Tris Buffered Saline	Beyotime,Shanghai	Cat# ST663
Sodium dodecyl sulfate(10%)	Beyotime,Shanghai	Cat# ST628
Ammonium persulfate substitute (APS substitute)	Beyotime,Shanghai	Cat# ST005
Tris base	Beyotime,Shanghai	Cat# ST789
Stripping buffer	Beyotime,Shanghai	Cat# P0025S
1.0M Tris-HCl pH6.8	DINGGUO,Beijing	Cat# WB-0021

REAGENT or RESOURCE	SOURCE	IDENTIFIER
30% acrylamide-bisacrylamide(29:1)	Beyotime,Shanghai	Cat# ST003
Ultra Pure Temed	invitrogen	Cat# 15524-010
Polyethylene glycol sorbitan monolaurate(Tween 20)	Beyotime,Shanghai	Cat# ST825
Methanol anhydrous	KESHI,Chengdu	CAS 67-56-1
Critical Commercial Assays		
DAB Substrate Kit	Abcam	Cat# ab64238
Enhanced BCA protein assay kit	Beyotime,Shanghai	Cat# P0010S
Amersham ECL prime luminol ehancer solution	GE	RPN2232V1
Experimental Models: Organisms/Strains		
Mouse: mT/mG	Jackson Laboratory	Cat#007676
Mouse: PLP-CreERT2	Jackson Laboratory	Cat#005795
Mouse: NG2-CreERT2	Jackson Laboratory	Cat#008538
Mouse: Tau-mGFP	Jackson Laboratory	Cat#021162
Mouse: APP/PS1	Jackson Laboratory	Cat#034832
Mouse: M1R fl/fl	Wang et al., 2018	N/A
Software and Algorithms		
SPSS (version 20.0)	IBM	https://www.ibm.com/analytics/spss-statistics-software RRID:SCR_019096
ZEN Digital Imaging for Light Microscopy	Zeiss	RRID:SCR_013672
Olympus Confocal Laser Scanning Microscope software	Olympus	RRID:SCR_017015
Imaris x64	Bitplane	http://www.bitplane.com/imaris/imaris; RRID: SCR_007370
ImageJ	NIH	https://imagej.nih.gov/ij/; RRID:SCR_003070
Image-Pro Plus software 5.0	Media Cybernetics	http://www.mediacy.com/imageproplus; RRID: SCR_007369
Other		
Champchem chem iluminscent image system	Sage Creation	610
Olympus Fluoview confocal microscope	Olympus	FV3000
Olympus IXplore SpinSR confocal microscope	Olympus	SpinSR
Zeiss Imager.M2 microscope	Zeiss	M2